Engineering with Computers (2022) 38 (Suppl 1):S353–S369
https://doi.org/10.1007/s00366-020-01152-2

ORIGINAL ARTICLE

On the phase velocity simulation of the multi curved viscoelastic system via an exact solution framework

M. S. H. Al-Furjan[1,2] · Masoud Mohammadgholiha[3] · Ibrahim M. Alarifi[4] · Mostafa Habibi[5,6] · Hamed Safarpour[7]

Received: 4 August 2020 / Accepted: 17 August 2020 / Published online: 3 September 2020

Abstract
The analysis of the wave propagation behavior of a sandwich structure with a soft core and multi-hybrid nanocomposite (MHC) face sheets is carried out in the framework of the higher-order shear deformation theory (HSDT). In order to take into account the viscoelastic influence, the Kelvin-Voight model is presented. In this paper, the constituent material of the core is made of an epoxy matrix which is reinforced by both macro- and nano-size reinforcements, namely carbon fiber (CF) and carbon nanotube (CNT). The effective material properties like Young's modulus or density are derived utilizing a micromechanical scheme incorporated with the Halpin–Tsai model. Then, on the basis of an energy-based Hamiltonian approach, the equations of motion are derived. The detailed parametric study is conducted, focusing on the combined effects of the viscoelastic foundation, CNT' weight fraction, core to total thickness ratio, small radius to total thickness ratio, and carbon fiber angle on the wave propagation behavior of sandwich structure. The results show that as well as increasing the phase velocity of the sandwich structure by increasing the wave number, this influence will be much more effective by increasing the damping factor. It is also observed that there is a critical value for the viscoelastic foundation that the relation between wave number and phase velocity will change from direct to indirect. The presented study outputs can be used in ultrasonic inspection techniques and structural health monitoring.

Keywords Kelvin-voight model · Multi-scale hybrid nanocomposite reinforcement · Elastic core · Doubly curved panel · Compatibility equations

1 Introduction

A key issue in the various engineering fields is that the prediction of the properties, behavior, and performance of different systems is an important aspect [1–12]. It is well knowen that the compositionally structures have a intresting thermo-electro-mechanical property and this matter is being an esential fact to get the attention of all engineering fields of reaserches for having efficient productions with the aid of composite structure, especially carbon-based nanofillers

✉ Mostafa Habibi
mostafahabibi@duytan.edu.vn

✉ Hamed Safarpour
Hamed_safarpor@yahoo.com

M. S. H. Al-Furjan
Rayan@hdu.edu.cn

Masoud Mohammadgholiha
m.mohamadgholiha@mail.kntu.ac.ir

Ibrahim M. Alarifi
i.alarifi@mu.edu.sa

1 School of Mechanical Engineering, Hangzhou Dianzi University, Hangzhou 310018, China

2 School of Materials Science and Engineering, State Key Laboratory of Silicon Materials, Zhejiang University, Hangzhou 310027, China

3 Department of Civil Engineering, K. N. Toosi University of Technology, Valiasr Street, P.O. Box 15875 4416, Tehran, Iran

4 Department of Mechanical and Industrial Engineering, College of Engineering, Majmaah University, Al-Majmaah, Riyadh 11952, Saudi Arabia

5 Institute of Research and Development, Duy Tan University, Da Nang 550000, Vietnam

6 Faculty of Electrical–Electronic Engineering, Duy Tan University, Da Nang 550000, Vietnam

7 Faculty of Engineering, Department of Mechanics, Imam Khomeini International University, Qazvin, Iran

reinforced structure [13–23]. In addition to whatwas mentioned owing to the wide applications of wave propagation analysis in structural health monitoring, most recently, an interesting field of research has been started in scholar which is called wave propagation response [24–29].

Based on the mentioned issue, Gao et al. [30] could report a mathematical framework to analyze the propagated wave in a GPLs reinforced porous FG plate via a well-known mixture method. Their results indicate that porosity and GPLs weight fraction are two important parameters in the field of structural health monitoring via wave propagation method. Ebrahimi et al. [31] were able to provide results on the characteristics of propagated waves in a compositionally nonlocal plate in which the structure located in a high-temperature environment. Also, they consider the shear deformation in each element of the structure; they found that without doubt the nonlocal effect has a bold role on the characteristics of propagated waves. Safaei et al. [32] tried to report characteristics of the propagated waves in a CNTs reinforced FG thermoelastic plate via the high-order ready plat theory and Mori–Tanaka method. Their important achievement was that the thermal stress and adding small amount of CNTs can make a remarkable effect on the wave velocity in the structure. Also, Many researches [22, 33–43] published the results of their investigation on the static and dynamic responses of the composite structures. By considering the mentioned necessities and in the field of wave propagation in composite beams and plates, Ebrahime et al. [44] could present a paper to investigate the wave propagation of the sandwich plate in which the structure is embedded in a nonlinear foundation. Also, they considered a magnetic environment in their model and used the classical theory for doing their computational formulation. Based on their results, the magnetic layer will play the most important role on the wave response of the sandwich plate [45]. presented a comprehensive formulation on the wave dispersion of a high-speed rotating 2D-FG nanobeam. They used nonlocal theory for consideration of the couple stress in the nanomechanics effect on the wave response of the structure. they could solve their complex formulation via an analytical method and they reported that the rotating speed is the most effective parameter. By employing the new version couple stress theory, Global matrix, and Legendre orthogonal polynomial methods, and, Liu et al. [46] had a try for reporting the characteristics of the propagated wave in a micro FG plate. They reported that by controlling the couple stress, we will have the grater phase velocity in the aspect of wave propagation. Ebrahimi et al. [47] succeeded in publishing a paper in which a computational framework is developed for investigation wave behavior in a thermally affected nonlocal beam which is made by FG materials. One of their assumptions was that the nanobeam is under high-speed rotation and is located in a thermal environment. They presented a lot of results, but the most significant one was that changing the rotating speed can provide some novel results on the wave propagation in the nanostructure. In a novel work, Barati [48] showed the behavior of propagated wave in the porous nanobeam with attention to the nonlocality via strain–stress gradient theory. Also, some researchers tried to predict the static and dynamic properties of different structures and materials via neural network solution [49–55].

In the scope of investigation of the wave dispertion in the smart structure, Li et al. [56] succeeded in publishing an article in which they examined the wave propagation of a smart plate via a semi-analytical method. They modeled a GPLs-reinforced plate which is covered with a piezoelectric actuator. They used the Reissner–Mindlin plate theory and Hamilton's principle for developing their computational approach and did the formulation. The application of their result is that GPLs in a matrix can play a positive role in structural health monitoring and improve wave propagation in the structures, especially smart structures. Ebrahimi et al. [57] developed a mathematical model for literature in which wave dispersion of a smart sandwich nanoplate by considering the nanosize effect via nonlocal strain gradient theory and the sandwich structure is made of ceramic face sheets and magnetostrictive core. Abad et al. [58] published an article in which they presented a formulation about the wave propagation problem of a somewhat sandwich thick plate. They smarted the plate by patching a piezoelectric layer on the top face of the structure and they considered Maxwell's assumptions in their computational approach. Habibi et al. [59] studied the wave response in a nanoshell with a GPLs reinforced compositionally core and patched piezoelectric face sheet. When they compared their result with molecular simulation can see that the nonlocality should be considered via NSGT. As a practical outcome they reported that the thickness of the smart layer will have more effect on the characteristics propagated waves in the nanoshell. Also, many studies reported the application of applied soft computing method for prediction of the behavior of complex system [60–67].

Based on the previous reaserch on the property of propagated waves in the cylandrical shell, Bakhtiari et al. [68] provided some results on the wave propagation of the FG shell in which fluid flow through the shell is considered. Ebrahimi et al. [69] studied the wave response in a high speed rotating nanoshell with a GPLs reinforced compositionally core and patched piezoelectric face sheet. They claimed that if the rotating should be controlled for improving the phase velocity of the nanoshell. The dispersion behavior of the wave in the MHC reinforced shell is investigated by Ebrahimi et al. [70]. They used the lowest order shear deformation theory and eigenvalue problem for providing their formulation and results. They found out the impact of nanosize reinforcements is more effective than the macro-size reinforcements for improving the phase velocity of the compositionally shell. Karami et al. [71] developed a mathematical model for literature in which wave dispersion in an imperfect nanoshell via NSG and HSD theories is analyzed. They provided some evidences that sensitivity of the prospected waves to the nonlocal effects, temperature, and humidity in the porous material should be considered. In addition, Stability of the complex structure is investigated in Refs [72, 73].

According to the summary of the presented paper in the literature, the analysis of the wave propagation behavior of a sandwich structure with a soft core and multi-hybrid nanocomposite (MHC) face sheets is carried out as a novel reaserch in the framework of the higher-order shear deformation theory (HSDT). In order to take into account, the viscoelastic influence, the Kelvin–Voight model is presented. In this paper, the constituent material of the core is made of an epoxy matrix which is reinforced by both macro- and nano-size reinforcements, namely carbon fiber (CF) and carbon nanotube (CNT). The effective material properties like Young's modulus or density are derived utilizing a micromechanical scheme incorporated with the Halpin–Tsai model. Then, on the basis of an energy-based Hamiltonian approach, the equations of motion are derived. The detailed parametric study is conducted, focusing on the combined effects of the viscoelastic foundation, CNT' weight fraction, core to total thickness ratio, small radius to total thickness ratio, and carbon fiber angle on the wave propagation behavior of sandwich structure.

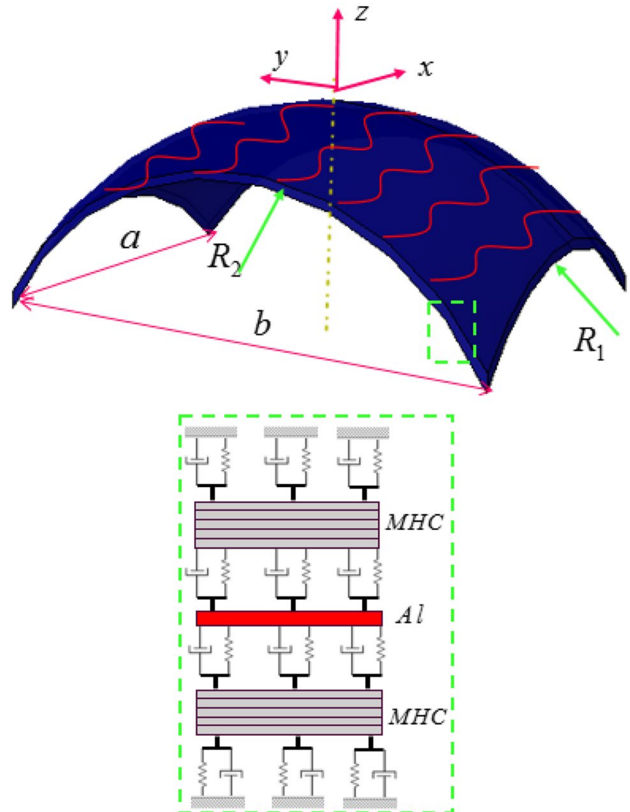

Fig. 1 A schematic of a sandwich doubly curved panel

2 Mathematical modeling

Figure 1 shows a sandwich doubly curved panel in a viscoelastic medium. The effective thickness ($h_b + h_c + h_t$) and the shell curvatures of the doubly curved panel are presented by h_{eff}, R_1, and R_2R, respectively. Besides, h_b h_c, and h_p are the thickness of the multi-hybrid nanocomposite reinforcement at the top layer, the core layer, and the multi-hybrid nanocomposite reinforcement at the bottom layer, respectively.

2.1 MHC Reinforcement

The procedure of homogenization is made of two main steps based upon the Halpin–Tsai model together with a micromechanical theory. The first stage is engaged with computing the effective characteristics of the composite reinforced with carbon fibers [74] as following [75]:

$$E_{11} = V_F E_{11}^F + V_{NCM} E^{NCM} \tag{1}$$

$$\frac{1}{E_{22}} = \frac{V_f}{E_{22}^F} + \frac{V_{NCM}}{E^{NCM}} - V_F V_{NCM} \times \frac{(v^F)^2 \frac{E^{NCM}}{E_{22}^F} + (v^{NCM})^2 \frac{E_{22}^F}{E^M} - 2v^F v^{NCM}}{V_F E_{22}^F + V_{NCM} E^{NCM}} \tag{2}$$

$$\frac{1}{G_{12}} = \frac{V_{NCM}}{G^{NCM}} + \frac{V_F}{G_{12}^F} \tag{3}$$

$$\rho = V_F \rho^F + V_{NCM} \rho^{NCM} \tag{4}$$

$$v_{12} = V_F v^F + V_{NCM} v^{NCM} \tag{5}$$

where elasticity modulus, mass density, Poisson's ratio, and shear modulus are symbolled via, and v. the superscripts of the matrix and fiber are *NCM* and *F*, respectively. Add the carbon fiber volume fraction (V_F) to the nanocomposite matrix volume fraction (V_{NCM}) is one.

$$V_F + V_{NCM} = 1 \tag{6}$$

The second step is organized to obtain the effective characteristics of the nanocomposite matrix reinforced with CNTs with the aid of the extended Halpin–Tsai micromechanics as follows:

$$E^j = \frac{5}{8}\left(\frac{1 + 2\beta_{dd} V_{CNT}}{1 - \beta_{dd} V_{CNT}}\right) E^M + \frac{3}{8}\left(\frac{\beta_{dl} V_{CNT}(2l^{CNT}/d^{CNT}) + 1}{1 - \beta_{dl} V_{CNT}}\right) \tag{7}$$

where β_{dd} and β_{dl} would be computed as the following expression:

$$\beta_{dl} = (E_{11}^{CNT}/E^M) - (d^{CNT}/4t^{CNT})/(E_{11}^{CNT}/E^M) + (l^{CNT}/2t^{CNT})$$
$$\beta_{dd} = (E_{11}^{CNT}/E^M) - (d^{CNT}/4t^{CNT})/(E_{11}^{CNT}/E^M) + (d^{CNT}/2t^{CNT}) \tag{8}$$

where volume fraction, thickness, length, elasticity modulus, weight fraction, and diameter of CNTs are V_{CNT}, t^{CNT}, l^{CNT}, E^{CNT},W_{CNT}, and d^{CNT}. Also, the volume fraction of the matrix and elasticity modulus of the matrix are V_M and E^M. So, The CNT volume fraction can be formulated as below:

$$V_{CNT}^{*} = \frac{W_{CNT}}{W_{CNT} + \left(\frac{\rho^{CNT}}{\rho^{M}}\right)\left(1 - W_{CNT}\right)} \tag{9}$$

Also, the effective volume fraction of CNTs can be formulated as follows:

$$\begin{aligned} V_{CNT} &= V_{CNT}^{*}\frac{\left|\xi_j\right|}{h}\ \text{FG} - \text{X} \\ V_{CNT} &= V_{CNT}^{*}\left(1 + \frac{2\xi_j}{h}\right)\ \text{FG} - \text{V} \\ V_{CNT} &= V_{CNT}^{*}\left(1 - \frac{2\xi_j}{h}\right)\ \text{FG} - \text{A} \\ V_{CNT} &= V_{CNT}^{*}\ \text{FG} - \text{UD} \end{aligned} \tag{10}$$

$$V_{CNT} + V_M = 1 \tag{11}$$

Also, Poisson's ratio, mass density, and shear modulus will be calculated as follows:

$$\rho^j = V_{CNT}\rho^{CNT} + V_M\rho^M \tag{12}$$

$$\nu^j = \nu^M \tag{13}$$

$$G^j = \frac{E^j}{2\left(1 + \nu^j\right)} \tag{14}$$

2.2 Kinematic relations

The displacement fields of the core can be given by [27, 76–81]:

$$\begin{aligned} u^c(x,y,z,t) &= u_0^c(x,y,t) + z_c\phi_x^c(x,y,t) - c_1 z_c^3\left[\phi_x^c(x,y,t) + \frac{\partial w_0^c(x,y,t)}{\partial x}\right] \\ v^c(x,y,z,t) &= v_0^c(x,y,t) + z_c\phi_y^c(x,y,t) - c_1 z_c^3\left[\phi_y^c(x,y,t) + \frac{\partial w_0^c(x,y,t)}{\partial y}\right] \\ w^c(x,y,z,t) &= w_0^c(x,y,t) \end{aligned} \tag{15}$$

The strain components can be given by

$$\begin{Bmatrix} \varepsilon_{xx}^c \\ \varepsilon_{yy}^c \\ \gamma_{xy}^c \\ \gamma_{xz}^c \\ \gamma_{yz}^c \end{Bmatrix} = \begin{bmatrix} \frac{\partial u_0^c}{\partial x} + z_c\frac{\partial \phi_x^c}{\partial x} - z_c^3 c_1\left(\frac{\partial \phi_x^c}{\partial x} + \frac{\partial^2 w_0^c}{\partial x^2}\right) + \frac{w_0^c}{R_1} \\ \frac{\partial v_0^c}{\partial y} + z_c\frac{\partial \phi_x^c}{\partial y} - z_c^3 c_1\left(\frac{\partial \phi_y^c}{\partial y} + \frac{\partial^2 w_0^c}{\partial y^2}\right) + \frac{w_0^c}{R_2} \\ \frac{\partial u_0^c}{\partial y} + \frac{\partial v_0^c}{\partial x} + z_c\left(\frac{\partial \phi_x^c}{\partial y} + \frac{\partial \phi_y^c}{\partial x}\right) - z_c^3 c_1\left(\frac{\partial \phi_x^c}{\partial y} + \frac{\partial \phi_y^c}{\partial x} + 2\frac{\partial^2 w_0^c}{\partial x \partial y}\right) \\ (1 - 3z_c^2 c_1)\left(\phi_x^c + \frac{\partial w_0^c}{\partial x}\right) \\ (1 - 3z_c^2 c_1)\left(\phi_y^c + \frac{\partial w_0^c}{\partial y}\right) \end{bmatrix} \tag{16}$$

where $\xi_j = \left(\frac{1}{2} + \frac{1}{2N_t} - \frac{j}{N_t}\right)h$ j = 1,2,...,N_t. Furthermore, the sum of V_M and V_{CNT} as the two constituents of the nanocomposite matrix is equal to 1.

Also, the strain–stress equations of the metal structure can be given as [24, 77, 82–92] follows:

$$\begin{bmatrix} \sigma_{xx}^c \\ \sigma_{yy}^c \\ \sigma_{xy}^c \\ \sigma_{xz}^c \\ \sigma_{yz}^c \end{bmatrix} = \begin{bmatrix} Q_{11} & Q_{12} & 0 & 0 & 0 \\ Q_{21} & Q_{22} & 0 & 0 & 0 \\ 0 & 0 & Q_{66} & 0 & 0 \\ 0 & 0 & 0 & Q_{55} & 0 \\ 0 & 0 & 0 & 0 & Q_{44} \end{bmatrix} \begin{bmatrix} \varepsilon_{xx}^c \\ \varepsilon_{yy}^c \\ \varepsilon_{xy}^c \\ \varepsilon_{xz}^c \\ \varepsilon_{yz}^c \end{bmatrix}, \tag{17}$$

in which [80, 93–99]

$$Q_{11} = Q_{22} = \frac{E_c}{1 - v_c^2}, \quad Q_{12} = Q_{21} = \frac{E_c v_c}{1 - v_c^2}, \quad Q_{44} = Q_{55} = Q_{66} = \frac{E_c}{2(1 + v_c)}$$

In Eq. (17) E_c, and v_c are Young's modulus and poison ratio of the metal, respectively.

2.3 Face sheets

In the present structural model for the sandwich panel, the HSDT is adopted for the face sheets. Hence, the displacement components of the top and bottom face sheets ($j = t, b$) are represented as follows:

$$\begin{aligned} u^j(x,y,z,t) &= u_0^j(x,y,t) + z_j\phi_x^j(x,y,t) - c_1 z_j^3\left[\phi_x^j(x,y,t) + \frac{\partial w_0^j(x,y,t)}{\partial x}\right] \\ v^j(x,y,z,t) &= v_0^j(x,y,t) + z\phi_y^j(x,y,t) - c_1 z_j^3\left[\phi_y^j(x,y,t) + \frac{\partial w_0^j(x,y,t)}{\partial y}\right] \\ w^j(x,y,z,t) &= w_0^j(x,y,t) \end{aligned} \tag{18}$$

The strain components can be given by [78, 83, 100–109]:

$$\begin{Bmatrix} \varepsilon_{xx}^j \\ \varepsilon_{yy}^j \\ \gamma_{xy}^j \\ \gamma_{xz}^j \\ \gamma_{yz}^j \end{Bmatrix} = \begin{bmatrix} \frac{\partial u_0^j}{\partial x} + z_j \frac{\partial \phi_x^j}{\partial x} - z_j^3 c_1 \left(\frac{\partial \phi_x^j}{\partial x} + \frac{\partial^2 w_0^j}{\partial x^2} \right) + \frac{w_0^j}{R_1} \\ \frac{\partial v_0^j}{\partial y} + z_j \frac{\partial \phi_x^j}{\partial y} - z_j^3 c_1 \left(\frac{\partial \phi_y^j}{\partial y} + \frac{\partial^2 w_0^j}{\partial y^2} \right) + \frac{w_0^j}{R_2} \\ \frac{\partial u_0^j}{\partial y} + \frac{\partial v_0^j}{\partial x} + z_j \left(\frac{\partial \phi_x^j}{\partial y} + \frac{\partial \phi_y^j}{\partial x} \right) - z_j^3 c_1 \left(\frac{\partial \phi_x^j}{\partial y} + \frac{\partial \phi_y^j}{\partial x} + 2\frac{\partial^2 w_0^j}{\partial x \partial y} \right) \\ (1 - 3z_j^2 c_1)\left(\phi_x^j + \frac{\partial w_0^j}{\partial x} \right) \\ (1 - 3z_j^2 c_1)\left(\phi_y^j + \frac{\partial w_0^j}{\partial y} \right) \end{bmatrix} \tag{19}$$

Also, the strain–stress equations of the metal structure can be given as [110–114]:

$$\begin{bmatrix} \sigma_{xx} \\ \sigma_{yy} \\ \sigma_{xy} \\ \sigma_{xz} \\ \sigma_{yz} \end{bmatrix}^j = \begin{bmatrix} \hat{\tilde{Q}}_{11}^j & \hat{\tilde{Q}}_{12}^j & 0 & 0 & \hat{\tilde{Q}}_{16}^j \\ \hat{\tilde{Q}}_{21}^j & \hat{\tilde{Q}}_{22}^j & 0 & 0 & \hat{\tilde{Q}}_{26}^j \\ 0 & 0 & \hat{\tilde{Q}}_{44}^j & \hat{\tilde{Q}}_{45}^j & 0 \\ 0 & 0 & \hat{\tilde{Q}}_{45}^j & \hat{\tilde{Q}}_{55}^j & 0 \\ \hat{\tilde{Q}}_{16}^j & \hat{\tilde{Q}}_{26}^j & 0 & 0 & \hat{\tilde{Q}}_{66}^j \end{bmatrix} \begin{bmatrix} \varepsilon_{xx} \\ \varepsilon_{yy} \\ \varepsilon_{xy} \\ \varepsilon_{xz} \\ \varepsilon_{yz} \end{bmatrix}^j, \tag{20}$$

where [115]

$$\hat{\tilde{Q}}_{11}^j = \cos^4\theta_f \tilde{Q}_{11}^j + 2\sin^2\theta_f \cos^2\theta_f \left(\tilde{Q}_{12}^j + 2\tilde{Q}_{66}^j \right) + \sin^4\theta_f \tilde{Q}_{22}^j \tag{21-a}$$

$$\hat{\tilde{Q}}_{12} = \sin^2\theta_f \cos^2\theta_f \left(\tilde{Q}_{11} + \tilde{Q}_{22} - 4\tilde{Q}_{66} \right) + \left(\sin^4\theta_f + \cos^4\theta_f \right) \tilde{Q}_{12} \tag{21-b}$$

$$\begin{aligned} \hat{\tilde{Q}}_{16} &= \cos^3\theta_f \sin\theta_f \left(2\tilde{Q}_{11} - 2\tilde{Q}_{12} - \tilde{Q}_{66} \right) \\ &+ \cos\theta_f \sin^3\theta_f \left(\tilde{Q}_{66} + 2\tilde{Q}_{12} - 2\tilde{Q}_{22} \right) \end{aligned} \tag{21-c}$$

$$\begin{aligned} \hat{\tilde{Q}}_{22} &= \sin^4\theta_f \tilde{Q}_{11} + 2\sin^2\theta_f \cos^2\theta_f \tilde{Q}_{12} \\ &+ \cos^4\theta_f \tilde{Q}_{22} + 2\sin^2\theta_f \cos^2\theta_f \left(\tilde{Q}_{12} + 2\tilde{Q}_{66} \right) \end{aligned} \tag{21-d}$$

$$\begin{aligned} \hat{\tilde{Q}}_{26} &= \cos^3\theta_f \sin\theta_f \left(2\tilde{Q}_{12} - 2\tilde{Q}_{22} + \tilde{Q}_{66} \right) \\ &+ \cos\ theta_f \sin^3\theta_f \left(2\tilde{Q}_{11} - 2\tilde{Q}_{12} - \tilde{Q}_{66} \right) \end{aligned} \tag{21-e}$$

$$Q^j_{11} = Q^j_{22} = \frac{E^j}{1-(\nu^j)^2},\quad Q^j_{12} = Q^j_{21} = \frac{E^j\nu^j}{1-(\nu^j)^2},\quad Q^j_{44} = Q^j_{55} = Q^j_{66} = \frac{E^j}{2(1+\nu^j)}$$

$$\hat{\hat{Q}}_{44} = \cos^2\theta_f\tilde{Q}_{44} + \sin^2\theta_f\tilde{Q}_{55}\hat{\hat{Q}}_{44} = \cos^2\theta_f\tilde{Q}_{44} + \sin^2\theta_f\tilde{Q}_{55} \tag{21-f}$$

$$\hat{\hat{Q}}_{45} = \cos\theta_f\sin\theta_f\left(\tilde{Q}_{55} - \tilde{Q}_{44}\right) \tag{21-g}$$

$$\hat{\hat{Q}}_{55} = \cos^2\theta_f\tilde{Q}_{55} + \sin^2\theta_f\tilde{Q}_{44} \tag{21-h}$$

$$\hat{\hat{Q}}_{66} = \tilde{Q}_{66}\left(\cos^2\theta_f - \sin^2\theta_f\right)^2 + 4\sin^2\theta_f\cos^2\theta_f\left(\tilde{Q}_{11} + \tilde{Q}_{22} - 2\tilde{Q}_{12}\right) \tag{21-i}$$

The terms involved in Eq. (21) would be obtained as follows:

2.4 Extended Hamilton's principle

For obtaining the governing equation and associated boundary conditions, we can apply Extended Hamilton's principle as follows [44, 70, 116, 117]:

$$\int_{t_1}^{t_2} (\delta U - \delta W)dt = 0 \tag{22}$$

The components of strain energy can be expressed as follows [24, 77, 90, 117–122]:

$$\delta U = \frac{1}{2}\left(\iiint_V \sigma^c_{mn}\delta\varepsilon^c_{mn}dV^c + \iiint_V \sigma^j_{mn}\delta\varepsilon^j_{mn}dV^j\right) =$$

$$= \iint_A \begin{bmatrix} N^c_{xx}\left(\frac{\partial\delta u^c_0}{\partial x} - \frac{\delta w^c_0}{R_1}\right) + M^c_{xx}\frac{\partial\delta\phi u^c_x}{\partial x} - P^c_{xx}c_1\left(\frac{\partial\delta\phi^c_x}{\partial x} + \frac{\partial^2\delta w^c_0}{\partial x^2}\right) \\ +N^c_{yy}\left(\frac{\partial\delta v^c_0}{\partial y} - \frac{\delta w^c_0}{R_2}\right) + M^c_{yy}\frac{\partial\delta\phi^c_x}{\partial y} - P^c_{yy}c_1\left(\frac{\partial\delta\phi^c_y}{\partial y} + \frac{\partial^2\delta w^c_0}{\partial y^2}\right) \\ +N^c_{xy}\frac{\partial\delta u^c_0}{\partial y} + N^c_{xy}\frac{\partial\delta v^c_0}{\partial x} + M^c_{xy}\left(\frac{\partial\delta\phi^c_x}{\partial y} + \frac{\partial\delta\phi^c_y}{\partial x}\right) \\ -P^c_{xy}c_1\left(\frac{\partial\delta\phi^c_x}{\partial y} + \frac{\partial\delta\phi^c_y}{\partial x} + 2\frac{\partial^2\delta w^c_0}{\partial x\partial y}\right) \\ +(Q^c_{xz} - 3S^c_{xz}c_1)\left(\delta\phi^c_x + \frac{\partial\delta w^c_0}{\partial x}\right) + (Q^c_{yz} - 3S^c_{yz}c_1)\left(\delta\phi^c_y + \frac{\partial\delta w^c_0}{\partial y}\right) \end{bmatrix}(1 + \frac{z^c}{R_1})(1 + \frac{z^c}{R_2})dA^c +$$

$$\iint_A \begin{bmatrix} N^j_{xx}\left(\frac{\partial\delta u^j_0}{\partial x} - \frac{\delta w^j_0}{R_1}\right) + M^j_{xx}\frac{\partial\delta\phi^j_x}{\partial x} - P^j_{xx}c_1\left(\frac{\partial\delta\phi^j_x}{\partial x} + \frac{\partial^2\delta w^j_0}{\partial x^2}\right) \\ +N^j_{yy}\left(\frac{\partial\delta v^j_0}{\partial y} - \frac{\delta w^j_0}{R_2}\right) + M^j_{yy}\frac{\partial\delta\phi^j_x}{\partial y} - P^j_{yy}c_1\left(\frac{\partial\delta\phi^j_y}{\partial y} + \frac{\partial^2\delta w^j_0}{\partial y^2}\right) \\ +N^j_{xy}\frac{\partial\delta u^j_0}{\partial y} + N^j_{xy}\frac{\partial\delta v^j_0}{\partial x} + M^j_{xy}\left(\frac{\partial\delta\phi^j_x}{\partial y} + \frac{\partial\delta\phi^j_y}{\partial x}\right) \\ -P^j_{xy}c_1\left(\frac{\partial\delta\phi^j_x}{\partial y} + \frac{\partial\delta\phi^j_y}{\partial x} + 2\frac{\partial^2\delta w_0}{\partial x\partial y}\right) \\ +(Q^j_{xz} - 3S^j_{xz}c_1)\left(\delta\phi^j_x + \frac{\partial\delta w^j_0}{\partial x}\right) + (Q^j_{yz} - 3S^j_{yz}c_1)\left(\delta\phi^j_y + \frac{\partial\delta w^j_0}{\partial y}\right) \end{bmatrix}(1 + \frac{z^j}{R_1})(1 + \frac{z^j}{R_2})dA^j \tag{23-a}$$

in which

$$
\begin{aligned}
&\left\{N_{xx}^{\lambda},N_{yy}^{\lambda},N_{xy}^{\lambda}\right\}=\int_{z_\lambda}\left\{\sigma_{xx}^{\lambda},\sigma_{yy}^{\lambda},\sigma_{xy}^{\lambda}\right\}dz_\lambda\\
&\left\{M_{xx}^{\lambda},M_{yy}^{\lambda},M_{xy}^{\lambda}\right\}=\int_{z_\lambda}\left\{\sigma_{xx}^{\lambda},\sigma_{yy}^{\lambda},\sigma_{xy}^{\lambda}\right\}z_\lambda dz_\lambda\\
&\left\{P_{xx}^{\lambda},P_{yy}^{\lambda},P_{xy}^{\lambda}\right\}=\int_{z_\lambda}\left\{\sigma_{xx}^{\lambda},\sigma_{yy}^{\lambda},\sigma_{xy}^{\lambda}\right\}z_\lambda^3 dz_\lambda\\
&\left\{Q_{xz}^{\lambda},Q_{yz}^{\lambda}\right\}=\int_{z_\lambda}\left\{\sigma_{xz}^{\lambda},\sigma_{xy}^{\lambda}\right\}dz_\lambda,\\
&\left\{S_{xz}^{\lambda},S_{yz}^{\lambda}\right\}=\int_{z_\lambda}\left\{\sigma_{xz}^{\lambda},\sigma_{xy}^{\lambda}\right\}z_\lambda^2 dz_\lambda
\end{aligned}
\tag{23-b}
$$

where $\lambda = b,\ t,\ c$. Also, the kinetic energy [123] of each layer of the structure can be defined as follows:

$$
\begin{aligned}
\delta K=&\int_{Z^j}\iint_{A^j}\rho^j\left\{\left(\frac{\partial u^j}{\partial t}\frac{\partial\delta u^j}{\partial t}\right)+\frac{\partial v^j}{\partial t}\frac{\partial\delta v^j}{\partial t}+\frac{\partial w^j}{\partial t}\frac{\partial\delta w^j}{\partial t}\right\}\left(1+\frac{z^j}{R_1}\right)\left(1+\frac{z^j}{R_2}\right)dA^j\\
&+\int_{Z^c}\iint_{A^c}\rho^c\left\{\left(\frac{\partial u^c}{\partial t}\frac{\partial\delta u^c}{\partial t}\right)+\frac{\partial v^c}{\partial t}\frac{\partial\delta v^c}{\partial t}+\frac{\partial w^c}{\partial t}\frac{\partial\delta w^c}{\partial t}\right\}\left(1+\frac{z^c}{R_1}\right)\left(1+\frac{z^c}{R_2}\right)dA^c
\end{aligned}
\tag{24}
$$

According to the Kelvin–Voight viscoelastic model for the MHC layer, the first variation of the viscoelastic model can be expressed as the following equation:

$$
\begin{aligned}
\delta W^c=&\iint_A K_w(2w^c\delta w^c-w^b\delta w^b-w^t\delta w^t)dA^c\\
&+C_d(2\dot{w}^c\delta\dot{w}^c-\dot{w}^b\delta\dot{w}^b-\dot{w}^t\delta\dot{w}^t)dA^c
\end{aligned}
\tag{25-a}
$$

Also, for piezoelectric layer, we have

$$
\delta W^j=\iint_{A^j}K_w(2w^j\delta w^j-w^c\delta w^c)dA^j+C_d(2\dot{w}^j\delta\dot{w}^j-\dot{w}^c\delta\dot{w}^c)dA^j
\tag{25-b}
$$

According to Eq. (25), K_w and C_d are elastic and dmping factor of the foundation.

Finally, the motion equations are derived as follows:

$$
\begin{aligned}
&\delta u_0^c:\ \frac{\partial N_{xx}^c}{\partial x}+\frac{\partial N_{xy}^c}{\partial y}=I_0^c\frac{\partial^2u_0^c}{\partial t^2}+I_1^c\frac{\partial^2\phi_x^c}{\partial t^2}-I_3^cc_1\left(\frac{\partial^2\phi_x^c}{\partial t^2}+\frac{\partial^3w_0^c}{\partial t^2\partial x}\right),\\
&\delta v_0^c:\ \frac{\partial N_{yy}^c}{\partial y}+\frac{\partial N_{xy}^c}{\partial x}=I_0^c\frac{\partial^2v_0^c}{\partial t^2}+I_1^c\frac{\partial^2\phi_y^c}{\partial t^2}-I_3^cc_1\left(\frac{\partial^2\phi_y^c}{\partial t^2}+\frac{\partial^3w_0^c}{\partial t^2\partial y}\right),\\
&\delta w_0^c:\ c_1\frac{\partial^2P_{xx}^c}{\partial x^2}+c_1\frac{\partial^2P_{yy}^c}{\partial y^2}+2c_1\frac{\partial^2P_{xy}^c}{\partial x\partial y}+\frac{\partial Q_{xz}^c}{\partial x}-3c_1\frac{\partial S_{xz}^c}{\partial x}+\frac{\partial Q_{yz}^c}{\partial y}-3c_1\frac{\partial S_{yz}^c}{\partial y}\\
&+\frac{N_{xx}^c}{R_1}+\frac{N_{yy}^c}{R_2}-K_w(2w^c\delta w^c-w^b\delta w^b-w^t\delta w^t)-C_d(2\dot{w}^c\delta\dot{w}^c-\dot{w}^b\delta\dot{w}^b-\dot{w}^t\delta\dot{w}^t)\\
&=c_1I_3^c\frac{\partial^3u_0}{\partial x\partial t^2}+\left(I_0^c\frac{\partial^2w_0^c}{\partial t^2}\right)+c_1I_3^c\frac{\partial^3v_y^c}{\partial y\partial t^2}+c_1I_3^c\frac{\partial^3\phi_y^c}{\partial y\partial t^2}-I_6^cc_1^2\left(\frac{\partial^3\phi_y^c}{\partial y\partial t^2}+\frac{\partial^4w_0^c}{\partial t^2\partial y^2}\right)\\
&+c_1I_4^c\frac{\partial^3\phi_x^c}{\partial x\partial t^2}-I_6^cc_1^2\left(\frac{\partial^3\phi_x^c}{\partial x\partial t^2}+\frac{\partial^4w_0^c}{\partial t^2\partial x^2}\right)\delta\phi_x^c:\ \frac{\partial M_{xx}^c}{\partial x}-c_1\frac{\partial P_{xx}^c}{\partial x}+\frac{\partial M_{xy}^c}{\partial y}-c_1\frac{\partial P_{xy}^c}{\partial y}-Q_{xz}^c+3c_1S_{xz}^c=\\
&+I_1^c\frac{\partial^2u_0}{\partial t^2}+I_2^c\frac{\partial^2\phi_x}{\partial t^2}-I_4^cc_1\left(\frac{\partial^2\phi_x}{\partial t^2}+\frac{\partial^3w}{\partial t^2\partial x}\right)\\
&-c_1I_3^c\frac{\partial^2u_0}{\partial t^2}-c_1I_4^c\frac{\partial^2\phi_x}{\partial t^2}+I_6^cc_1^2\left(\frac{\partial^2\phi_x^c}{\partial t^2}+\frac{\partial^3w_0^c}{\partial t^2\partial x}\right)\delta\phi_y^c:\ \frac{\partial M_{yy}^c}{\partial y}-c_1\frac{\partial P_{yy}^c}{\partial y}+\frac{\partial M_{xy}^c}{\partial x}-c_1\frac{\partial P_{xy}^c}{\partial x}-Q_{yz}^c+3c_1S_{yz}^c=\\
&I_1^c\frac{\partial^2v_0}{\partial t^2}+I_2^c\frac{\partial^2\phi_y}{\partial t^2}-I_4^cc_1\left(\frac{\partial^2\phi_y^c}{\partial t^2}+\frac{\partial^3w_0^c}{\partial t^2\partial y}\right)-c_1I_3^c\frac{\partial^2v_0}{\partial t^2}-c_1I_4^c\frac{\partial^2\phi_y}{\partial t^2}+I_6^cc_1^2\left(\frac{\partial^2\phi_y^c}{\partial t^2}+\frac{\partial^3w_0^c}{\partial t^2\partial y}\right)
\end{aligned}
\tag{26}
$$

Also, the motion equations for the nanocomposite face sheets are as follows:

$$
\begin{aligned}
&\delta u_0^j : \frac{\partial N_{xx}^j}{\partial x} + \frac{\partial N_{xy}^j}{\partial y} = I_0^j \frac{\partial^2 u_0^j}{\partial t^2} + I_1^j \frac{\partial^2 \phi_x^j}{\partial t^2} - I_3^j c_1 \left(\frac{\partial^2 \phi_x^j}{\partial t^2} + \frac{\partial^3 w_0^j}{\partial t^2 \partial x} \right), \\
&\delta v_0^j : \frac{\partial N_{yy}^j}{\partial y} + \frac{\partial N_{xy}^j}{\partial x} = I_0^j \frac{\partial^2 v_0^j}{\partial t^2} + I_1^j \frac{\partial^2 \phi_y^j}{\partial t^2} - I_3^j c_1 \left(\frac{\partial^2 \phi_y^j}{\partial t^2} + \frac{\partial^3 w_0^j}{\partial t^2 \partial y} \right), \\
&\delta w_0^j : c_1 \frac{\partial^2 P_{xx}^j}{\partial x^2} + c_1 \frac{\partial^2 P_{yy}^j}{\partial y^2} + 2c_1 \frac{\partial^2 P_{xy}^j}{\partial x \partial y} + \frac{\partial Q_{xz}^j}{\partial x} - 3c_1 \frac{\partial S_{xz}^j}{\partial x} + \frac{\partial Q_{yz}^j}{\partial y} - 3c_1 \frac{\partial S_{yz}^j}{\partial y} \\
&+ \frac{N_{xx}^j}{R_1} + \frac{N_{yy}^j}{R_2} - K_w(2w^j - w^c) - C_d(2\dot{w}^j - \dot{w}^c) = c_1 I_3^j \frac{\partial^3 u_0^j}{\partial x \partial t^2} + c_1 I_4^j \frac{\partial^3 \phi_x^j}{\partial x \partial t^2} + \left(I_0^j \frac{\partial^2 w_0^j}{\partial t^2} \right) \\
&+ c_1 I_3^j \frac{\partial^3 v_0^j}{\partial y \partial t^2} + c_1 I_4^j \frac{\partial^3 \phi_y^j}{\partial y \partial t^2} - I_6^j c_1^2 \left(\frac{\partial^3 \phi_y^j}{\partial y \partial t^2} + \frac{\partial^4 w_0^j}{\partial t^2 \partial y^2} \right) - I_6^j c_1^2 \left(\frac{\partial^3 \phi_x^j}{\partial x \partial t^2} + \frac{\partial^4 w_0^j}{\partial t^2 \partial x^2} \right) \\
&\delta \phi_x^j : \frac{\partial M_{xx}^j}{\partial x} - c_1 \frac{\partial P_{xx}^j}{\partial x} + \frac{\partial M_{xy}^j}{\partial y} - c_1 \frac{\partial P_{xy}^j}{\partial y} - Q_{xz}^j + 3c_1 S_{xz}^j = \\
&+ I_1^j \frac{\partial^2 u_0^j}{\partial t^2} + I_2^j \frac{\partial^2 \phi_x^j}{\partial t^2} - I_4^j c_1 \left(\frac{\partial^2 \phi_x^j}{\partial t^2} + \frac{\partial^3 w_0^j}{\partial t^2 \partial x} \right) \\
&- c_1 I_3^j \frac{\partial^2 u_0^j}{\partial t^2} - c_1 I_4^j \frac{\partial^2 \phi_x^j}{\partial t^2} + I_6^j c_1^2 \left(\frac{\partial^2 \phi_x^j}{\partial t^2} + \frac{\partial^3 w_0^j}{\partial t^2 \partial x} \right) \\
&\delta \phi_y^j : \frac{\partial M_{yy}^j}{\partial y} - c_1 \frac{\partial P_{yy}^j}{\partial y} + \frac{\partial M_{xy}^j}{\partial x} - c_1 \frac{\partial P_{xy}^j}{\partial x} - Q_{yz}^j + 3c_1 S_{yz}^j = \\
&I_1^j \frac{\partial^2 v_0^j}{\partial t^2} + I_2^j \frac{\partial^2 \phi_y^j}{\partial t^2} - I_4^j c_1 \left(\frac{\partial^2 \phi_y^j}{\partial t^2} + \frac{\partial^3 w_0^j}{\partial t^2 \partial y} \right) \\
&- c_1 I_3^j \frac{\partial^2 v_0^j}{\partial t^2} - c_1 I_4^j \frac{\partial^2 \phi_y^j}{\partial t^2} + I_6^j c_1^2 \left(\frac{\partial^2 \phi_y^j}{\partial t^2} + \frac{\partial^3 w_0^j}{\partial t^2 \partial y} \right) \delta u_0^j : \frac{\partial N_{xx}^j}{\partial x} + \frac{\partial N_{xy}^j}{\partial y} = I_0^j \frac{\partial^2 u_0^j}{\partial t^2} + I_1^j \frac{\partial^2 \phi_x^j}{\partial t^2} - I_3^j c_1 \left(\frac{\partial^2 \phi_x^j}{\partial t^2} + \frac{\partial^3 w_0^j}{\partial t^2 \partial x} \right), \\
&\delta v_0^j : \frac{\partial N_{yy}^j}{\partial y} + \frac{\partial N_{xy}^j}{\partial x} = I_0^j \frac{\partial^2 v_0^j}{\partial t^2} + I_1^j \frac{\partial^2 \phi_y^j}{\partial t^2} - I_3^j c_1 \left(\frac{\partial^2 \phi_y^j}{\partial t^2} + \frac{\partial^3 w_0^j}{\partial t^2 \partial y} \right), \\
&\delta w_0^j : c_1 \frac{\partial^2 P_{xx}^j}{\partial x^2} + c_1 \frac{\partial^2 P_{yy}^j}{\partial y^2} + 2c_1 \frac{\partial^2 P_{xy}^j}{\partial x \partial y} + \frac{\partial Q_{xz}^j}{\partial x} - 3c_1 \frac{\partial S_{xz}^j}{\partial x} + \frac{\partial Q_{yz}^j}{\partial y} - 3c_1 \frac{\partial S_{yz}^j}{\partial y} \\
&+ \frac{N_{xx}^j}{R_1} + \frac{N_{yy}^j}{R_2} - K_w(2w^j - w^c) - C_d(2\dot{w}^j - \dot{w}^c) = c_1 I_3^j \frac{\partial^3 u_0^j}{\partial x \partial t^2} + c_1 I_4^j \frac{\partial^3 \phi_x^j}{\partial x \partial t^2} + \left(I_0^j \frac{\partial^2 w_0^j}{\partial t^2} \right) \\
&+ c_1 I_3^j \frac{\partial^3 v_0^j}{\partial y \partial t^2} + c_1 I_4^j \frac{\partial^3 \phi_y^j}{\partial y \partial t^2} - I_6^j c_1^2 \left(\frac{\partial^3 \phi_y^j}{\partial y \partial t^2} + \frac{\partial^4 w_0^j}{\partial t^2 \partial y^2} \right) - I_6^j c_1^2 \left(\frac{\partial^3 \phi_x^j}{\partial x \partial t^2} + \frac{\partial^4 w_0^j}{\partial t^2 \partial x^2} \right) \\
&\delta \phi_x^j : \frac{\partial M_{xx}^j}{\partial x} - c_1 \frac{\partial P_{xx}^j}{\partial x} + \frac{\partial M_{xy}^j}{\partial y} - c_1 \frac{\partial P_{xy}^j}{\partial y} - Q_{xz}^j + 3c_1 S_{xz}^j = \\
&+ I_1^j \frac{\partial^2 u_0^j}{\partial t^2} + I_2^j \frac{\partial^2 \phi_x^j}{\partial t^2} - I_4^j c_1 \left(\frac{\partial^2 \phi_x^j}{\partial t^2} + \frac{\partial^3 w_0^j}{\partial t^2 \partial x} \right) \\
&- c_1 I_3^j \frac{\partial^2 u_0^j}{\partial t^2} - c_1 I_4^j \frac{\partial^2 \phi_x^j}{\partial t^2} + I_6^j c_1^2 \left(\frac{\partial^2 \phi_x^j}{\partial t^2} + \frac{\partial^3 w_0^j}{\partial t^2 \partial x} \right) \\
&\delta \phi_y^j : \frac{\partial M_{yy}^j}{\partial y} - c_1 \frac{\partial P_{yy}^j}{\partial y} + \frac{\partial M_{xy}^j}{\partial x} - c_1 \frac{\partial P_{xy}^j}{\partial x} - Q_{yz}^j + 3c_1 S_{yz}^j = \\
&I_1^j \frac{\partial^2 v_0^j}{\partial t^2} + I_2^j \frac{\partial^2 \phi_y^j}{\partial t^2} - I_4^j c_1 \left(\frac{\partial^2 \phi_y^j}{\partial t^2} + \frac{\partial^3 w_0^j}{\partial t^2 \partial y} \right) \\
&- c_1 I_3^j \frac{\partial^2 v_0^j}{\partial t^2} - c_1 I_4^j \frac{\partial^2 \phi_y^j}{\partial t^2} + I_6^j c_1^2 \left(\frac{\partial^2 \phi_y^j}{\partial t^2} + \frac{\partial^3 w_0^j}{\partial t^2 \partial y} \right)
\end{aligned}
\tag{27}
$$

where

$$\left\{I_0^j, I_1^j, I_2^j, I_3^j\right\} = \int_{-\frac{h}{2}}^{\frac{h}{2}} \rho\{1, z, z^2, z^3\}(1 + \frac{z}{R_1})(1 + \frac{z}{R_2})dz \quad (28)$$

2.5 Solution procedure

Displacement fields for investigation the wave propagation analysis of the structure are defined as follows [117]:

$$\begin{Bmatrix} u_0^c \\ v_0^c \\ w_0^c \\ \phi_x^c \\ \phi_y^c \end{Bmatrix} = \begin{Bmatrix} U_0^c \exp(sx + n\theta - \omega t)i \\ V_0^c \exp(sx + n\theta - \omega t)i \\ W_0^c \exp(sx + n\theta - \omega t)i \\ \Phi_x^c \exp(sx + n\theta - \omega t)i \\ \Phi_y^c \exp(sx + n\theta - \omega t)i \end{Bmatrix}, \begin{Bmatrix} u_0^j \\ v_0^j \\ w_0^j \\ \phi_x^j \\ \phi_y^j \end{Bmatrix} = \begin{Bmatrix} U_0^j \exp(sx + n\theta - \omega t)i \\ V_0^j \exp(sx + n\theta - \omega t)i \\ W_0^j \exp(sx + n\theta - \omega t)i \\ \Phi_x^j \exp(sx + n\theta - \omega t)i \\ \Phi_y^j \exp(sx + n\theta - \omega t)i \end{Bmatrix}, \quad (29)$$

where s and n are wave numbers along with the directions of x and y, respectively; also ω is called frequency. With replacing Eq. (29) into governing equations we get:

$$([K] - \omega^2[M])\{d\} = \{0\} \quad (30)$$

where

$$\{d\} = \left\{ u_0 \ v_0 \ w_0 \ \psi_{x_0} \ \psi_{\theta_0} \right\} \quad (31)$$

Also, the phase velocity of wave dispersion can be calculated by Eq. (32):

$$c = \frac{\omega}{s} \quad (32)$$

In Eq. (32),c and s are called phase velocity and wavenumber of a laminated nanocomposite cylindrical shell, respectively. These parameters are propagation speeds of the particles in a sandwich panel.

Table 1 Comparison of the first dimensionless natural frequency of simply supported CNT reinforced composite square perfect panel (a/h = 10)

V_{CNT}	Ref [31]	Ref [32]	Present study
11%	0.1319	0.1357	0.1350
14%	0.1400	0.1438	0.1429
17%	0.1638	0.1685	0.1658

2.6 Validation

The obtained results for the perfect panel are compared with the results of Refs. [124, 125]. These results are listed in Table 1. From this table, it can be seen that the present results have a good agreement with the obtained results in the literature. Note that, the dimensionless form of the frequency can be calculated using the following relation:

$$\Omega = \Omega\frac{a^2}{h}\sqrt{\frac{\rho_M}{E_M}} \quad (33)$$

For more verification, the fundamental frequencies of the FML moderately thick plates resting on partial elastic foundations are calculated by eigenvalue problem. In Table 2, non-dimensional fundamental frequencies of the symmetrically laminated cross-ply plate $(0^\circ, 90^\circ, 90^\circ, 0^\circ)$ are shown as compared for different E_1/E_2.

3 Results

In this part, a comprehensive investigation is carried out to demonstrate the effects of various parameters on the phase velocity response of a multi-hybrid nanocomposite doubly curved panel. The geometrical and material characteristics of constituent materials would be presented in Table 3. Also, the material properties of aluminum properties can be given as follows:$E = 3.51\,GPa, \quad \rho = 1200kg/m^3, \quad \nu = 0.34$.

Figure 2 is presented for investigating the influence of the damping factor of the foundation on the characteristic of the elastic propagating wave. Figure 2 shows that as well as

Table 2 Non-dimensional fundamental frequency of simply supported cross-ply laminated square plate with $G_{12}/E_2 = 0.6$, $G_{13}/E_2 = 0.6$, $G_{23}/E_2 = 0.5$, a = b = 1, υ=0.25

E_1/E_2	Ref [33]	Ref [34]	Presented study	Discrepancy
10	8.2982	8.2981	8.5485	3%
20	9.5671	9.5671	10.0328	4%
30	10.326	10.326	10.6318	2%
40	10.824	10.854	11.0045	1%

Table 3 Material properties of the multiscale hybrid nanocomposite annular plate [33]

Carbon fiber	E_{11}^F	E_{22}^F	G_{12}^F	ρ^F	ν^F	α_{11}^F	α_{22}^F		
	[Gpa]	[Gpa]	[Gpa]	[kg/m^3]		[$\times 10^{-6}/k$]	[$\times 10^{-6}/k$]		
	233.05	23.1	8.96	1750	0.2	− 0.54	10.08		
Epoxy Matrix	E^m	ν^m		ρ^m		α^m			
	[Gpa]			[kg/m^3]		[$\times 10^{-6}$/k]			
	3.51	0.34		1200		45			
Carbon nanotube	d^{CNT}	l^{CNT}	ρ^{CNT}	$G_{12}^{CNT} = G_{13}^{CNT}$	$E_{22}^{CNT} = E_{33}^{CNT}$	ρ^m	t^{CNT}	d^{CNT}	t^{CNT}
	[nm]	[μm]	[kg/m^3]	[Tpa]	[Tpa]	[kg/m^3]	[nm]	[nm]	[nm]
	1.4	25	1350	1.9445	7.0800	1200	0.34	1.4	0.34

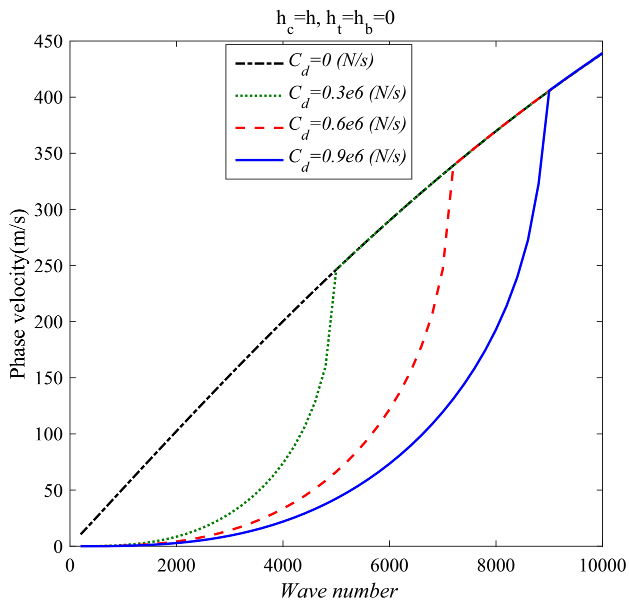

Fig. 2 The phase velocity versus wavenumber for four value of C_d

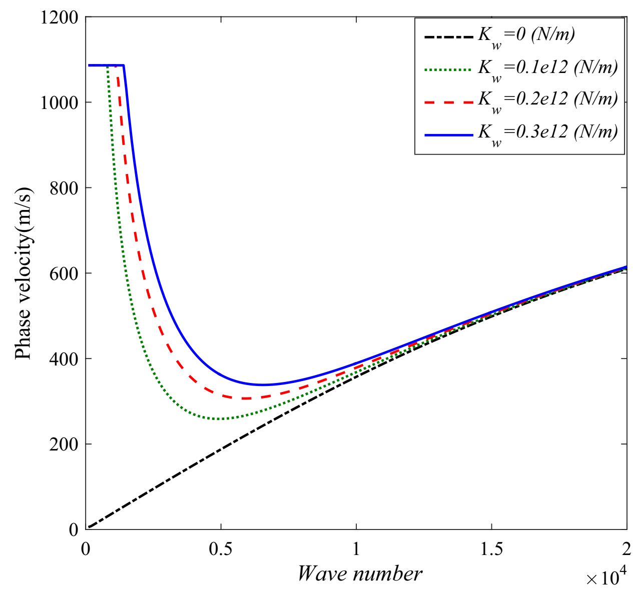

Fig. 3 The effect of the elastic parameter of the foundation on the characteristic of the propagated wave in the FML panel

increasing the phase velocity of the FML panel by increasing the wavenumber, this influence will be much more effective by increasing the damping factor. Also, at the grater wave number, we cannot find any change in the wave behavior of the sandwich panel due to increasing the damping factor. As the most impressive result, by improving the elastic foundation the ineffective range of the wavenumber will be limited in which there is not any effect from C_d of the foundation on the phase velocity. Initially, as the wave number increases, the phase velocity of the panel increases, exponentially, while the relation between phase velocity and wave number is linear at the grater wave number. Last but not the least, as C_d increase, the phase velocity improves. In Fig. 3 the phase velocity of the hybrid nanocomposite doubly curved panel versus wave number is presented with attention to the effect of elastic parameter (K_w) of the foundation. Base on Fig. 3 can conclude that when the elastic parameter of the foundation is considered zero, as the wave number increases, the phase velocity improves, logarithmic while this relation will be complex by considering $K_w > 0$. For each K_w, at first, the phase velocity of the panel is constant by increasing the wavenumber, and at the medium values of the wavenumber, the phase velocity will be falling, so after a minimum value the relation changes to be increasing. Another important result from Fig. 3 is that the impact of K_w on the wave response of the structure is considerable for $0.1 < K_w e4 < 0.8$, and this effect from the elastic foundation on the phase velocity could be negligible at the initial and grate value of the wavenumber. Figure 4 is presented for investigating the influence of elastic factor of the foundation and core to total thickness (h_c/h) on the characteristic of the propagate elastic wave. As stated by Fig. 4 the impact of K_w on the phase velocity is more obvious and considerable if the h_c/h is between 0.5 to 0.8. in other words, the phase velocity can

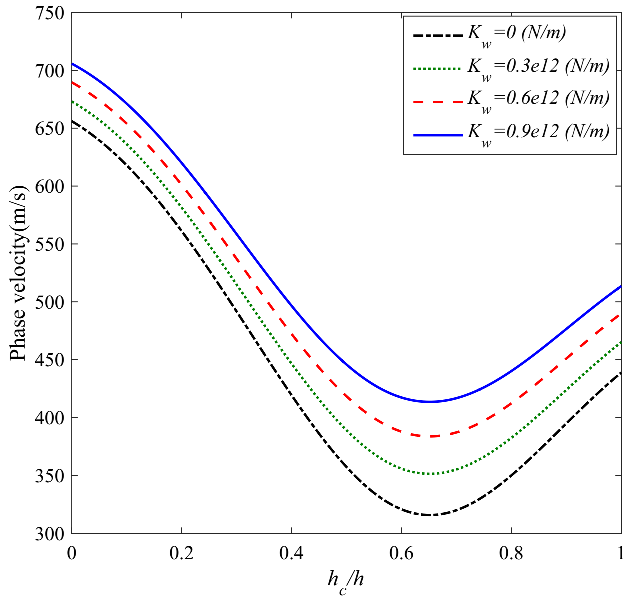

Fig. 4 The phase velocity versus h_c/h with having attention to the impact of K_w

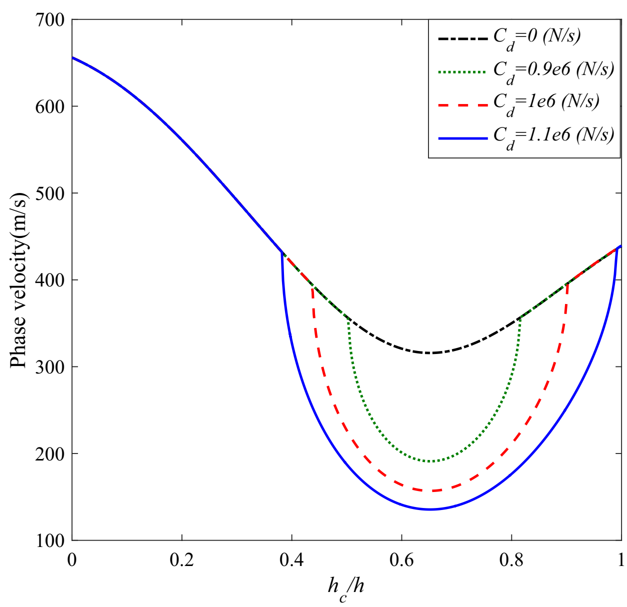

Fig. 5 The phase velocity versus h_c/h with having attention to the impact of C_d

improve due to increasing the K_w and this enhancement will be more considerable for $0.5 \le h_c/h \le 0.8$. In addition, it is true that when the thickness of the core is small the phase velocity is falling down owing to increasing the h_c/h, but if we consider the thicker core, we can find a direct relation between h_c/h and phase velocity Figs 5, 6, 7 and 8.

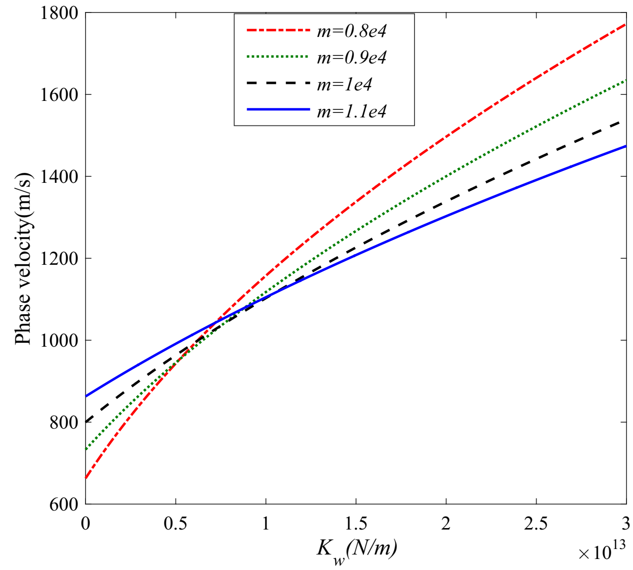

Fig. 6 The phase velocity versus K_w with having attention to the impact of wavenumber

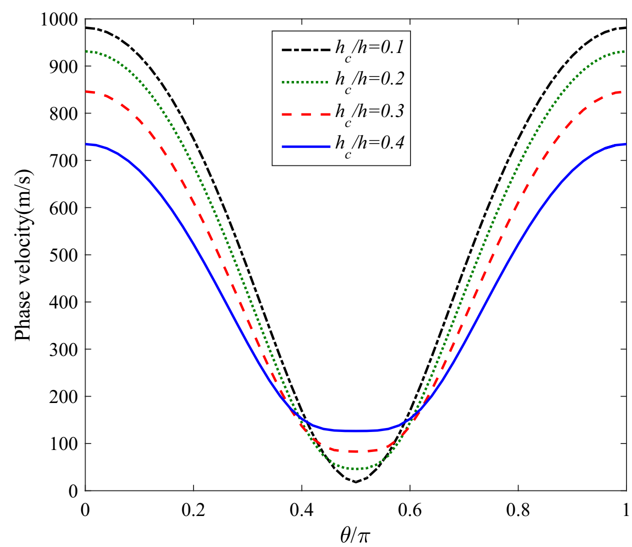

Fig. 7 The phase velocity versus θ/π with having attention to the impact of h_c/h

With close attention to the provided diagrams in Fig. 9 we can see that as well as an improvement on the phase velocity of the structure due to increasingK_w, the mentioned impact is more remarkable when the carbon fibers in the matrix are distributed vertically. In addition, if the fibers are vertical, there is not any change in the phase velocity due to any change inθ/π. The main point of Fig. 9 is that the wave response of the MHC reinforced panel is more dependent on the carbon fiber angle and the impact of the elastic factor of the foundation on the phase velocity is more effective when

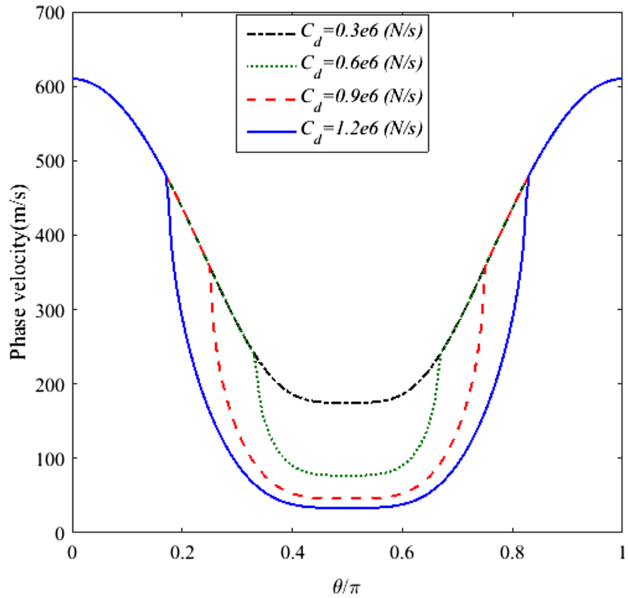

Fig. 8 The phase velocity versus θ/π with having attention to the impact of C_d

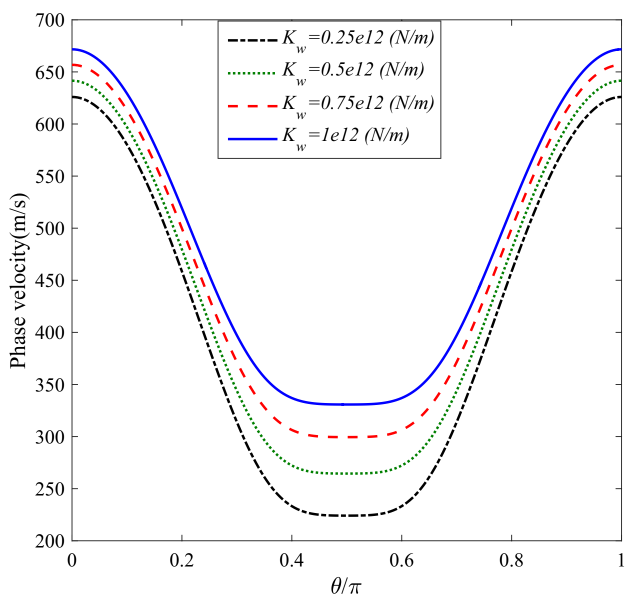

Fig. 9 The phase velocity versus θ/π with having attention to the impact of the elastic factor of the foundation

the fiber angle is vertical. Reported data in Fig. 10 are shown to have a deep presentation about the effects of the carbon fiber angle (θ/π)and CNT weight fraction (W_{CNT}) on the wave responses of the sandwich structure. The most general result in Fig. 10 is that for eachW_{CNT}, when the fiber angle is

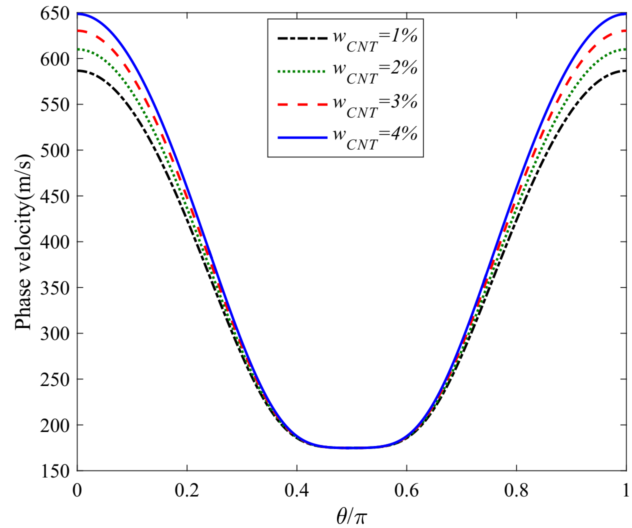

Fig. 10 The phase velocity versus θ/π with having attention to the impact of the elastic factor of the foundation

less than$\pi/2$, the phase velocity is decreasing and this trend will be reverse for the fiber angle more than$\pi/2$. The most interesting result in

Fig. 10 is that when the fiber angle is $0.4 \le \theta/\pi \le 0.6$, adding more CNTs cannot provide any change on the phase velocity of the structure. As another explanation, if the fibers are distributed in the matrix vertically, changing W_{CNT} cannot play any role on the wave response of the sandwich panel and as the fibers become horizontal, the effect of the W_{CNT} on the phase velocity becomes more dramatic. Provided diagrams in Fig. 11 are shown to have a comparative study about the effects of elastic and damping factors (K_w andC_d) of the foundation on the wave responses of the doubly carved smart panel. The most principal result from Fig. 11 is that in the (K_w, C_d) plane, there is a region as the same as a trapezium in which there are no effects from elastic and damping factors of the foundation on the wave response of the sandwich smart panel and this area will be small by increasing the value of wavenumber. The last and impressive outcome is that the effect of C_d on the phase velocity is greater than the impact of K_w on the wave propagation of the panel. The reported 3D diagram in Fig. 12 is shown in order to have a comparative study about the effects of the wavenumber and fiber angle on the wave responses of the doubly carved panel. The most principal and evident result in Fig. 12 is that as the wave number increases, the changes in phase velocity of the sandwich panel which is caused by increasing the fibers angel becomes much more dramatic. In the simpler words, the effects of fiber angle on the phase velocity of the FML panel is highly dependent on the wavenumber.

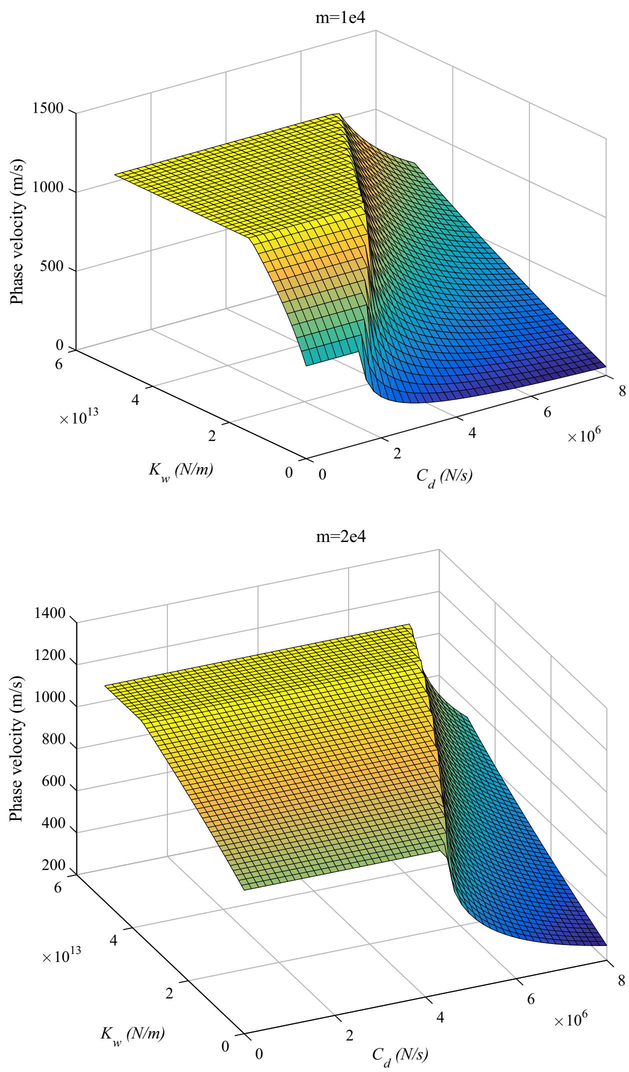

Fig. 11 The impacts of K_w and C_d on the wave response of the sandwich smart panel

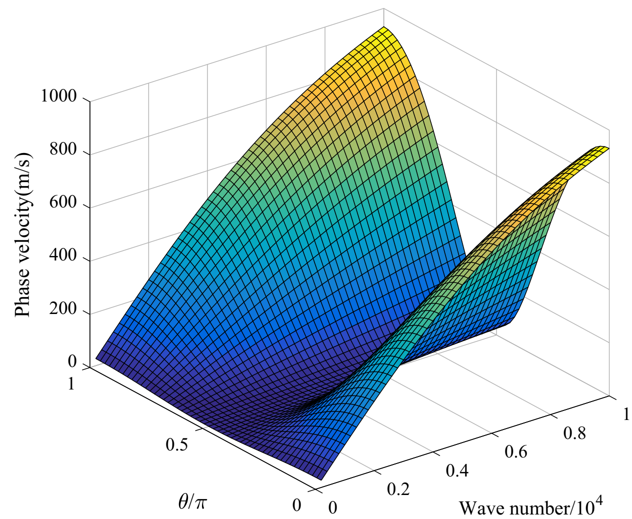

Fig. 12 The phase velocity of the panel with respect to the impact of wavenumber and fiber angie

4 Conclusion

The analysis of the wave propagation behavior of a sandwich structure with a soft core and multi-hybrid nanocomposite (MHC) face sheets is carried out as a novel reaserch in the framework of the higher-order shear deformation theory (HSDT). In order to take into account the viscoelastic influence, the Kelvin-Voight model is presented. In this paper, the constituent material of the core is made of an epoxy matrix which is reinforced by both macro- and nano-size reinforcements, namely carbon fiber (CF) and carbon nanotube (CNT). The effective material properties like Young's modulus or density are derived utilizing a micromechanical scheme incorporated with the Halpin–Tsai model. Then, on the basis of an energy-based Hamiltonian approach, the equations of motion are derived. Finally, the most bolded results of this paper are as follow:

As well as increasing the phase velocity of the FML panel by increasing the wavenumber, this influence will be much more effective by increasing the damping factor;

By improving the elastic foundation the ineffective range of the wavenumber will be limited in which there is not any effect from C_d of the foundation on the phase velocity;

K_w=8e12 is a critical value for the viscoelastic foundation that the relation between wavenumber and phase velocity will change from direct to indirect;

When the orientation of the carbon fiber in the matrix is being close to the vertical axis, the effect of C_d on the phase velocity of the sandwich panel will be evident and this impact is a positive point for increasing the wave propagation response of the panel;

In a specific range of θ/π, the damping factor of the foundation has an ineffective role on the phase velocity of the panel and the range will be small by boosting the C_d;

If the fibers are distributed in the matrix vertically, changing W_{CNT} cannot play any role on the wave response of the sandwich panel and as the fibers become horizontal, the effect of the W_{CNT} on the phase velocity becomes more dramatic;

The effects of fiber angel on the phase velocity of the FML panel is hardly dependent on the wavenumber.

Funding National Natural Science Foundation of China (51675148). The Outstanding Young Teachers Fund of Hangzhou Dianzi University (GK160203201002/003). National Natural Science Foundation of China (51805475).

References

1. Gao N-S, Guo X-Y, Cheng B-Z, Zhang Y-N, Wei Z-Y, Hou H (2019) Elastic wave modulation in hollow metamaterial beam with acoustic black hole. IEEE Access 7:124141–124146
2. Gao N, Wei Z, Zhang R, Hou H (2019) Low-frequency elastic wave attenuation in a composite acoustic black hole beam. Appl Acous 154:68–76
3. Gao N, Zhang Y (2019) A low frequency underwater metastructure composed by helix metal and viscoelastic damping rubber. J Vibr Control 25(3):538–548
4. Gao N, Hou H, Wu JH (2018) A composite and deformable honeycomb acoustic metamaterial. Int J Modern Phys B 32(20):1850204
5. Gao N, Wu JH, Yu L, Hou H (2016) Ultralow frequency acoustic bandgap and vibration energy recovery in tetragonal folding beam phononic crystal. Int J Modern Phys B 30(18):1650111
6. Tian X, Song Z, Wang J (2019) Study on the propagation law of tunnel blasting vibration in stratum and blasting vibration reduction technology. Soil Dynam Earthquake Eng 126:105813
7. Mou B, Bai Y, Patel V (2020) Post-local buckling failure of slender and over-design circular CFT columns with high-strength materials. Eng Str 210:110197
8. Guo C, Hu M, Li Z, Duan F, He L, Zhang Z, Marchetti F, Du M (2020) Structural hybridization of bimetallic zeolitic imidazolate framework (ZIF) nanosheets and carbon nanofibers for efficiently sensing α-synuclein oligomers. Sens Actuat B Chem 309:127821
9. Mou B, Li X, Qiao Q, He B, Wu M (2019) Seismic behaviour of the corner joints of a frame under biaxial cyclic loading. Eng Str 196:109316
10. Mou B, Zhao F, Qiao Q, Wang L, Li H, He B, Hao Z (2019) Flexural behavior of beam to column joints with or without an overlying concrete slab. Eng Str 199:109616
11. Luo X, Guo J, Chang P, Qian H, Pei F, Wang W, Miao K, Guo S, Feng G (2020) ZSM-5@ MCM-41 composite porous materials with a core-shell structure: Adjustment of mesoporous orientation basing on interfacial electrostatic interactions and their application in selective aromatics transport. Separ Purif Technol 239:116516
12. Chen H, Zhang G, Fan D, Fang L, Huang L (2020) Nonlinear lamb wave analysis for microdefect identification in mechanical structural health assessment. Measurement 29:108026. https://doi.org/10.1016/j.measurement.2020.108026
13. Bourada F, Bousahla AA, Tounsi A, Bedia E, Mahmoud S, Benrahou KH, Tounsi A (2020) Stability and dynamic analyses of SW-CNT reinforced concrete beam resting on elastic-foundation. Computers Concrete 25(6):485–495
14. Matouk H, Bousahla AA, Heireche H, Bourada F, Bedia E, Tounsi A, Mahmoud S, Tounsi A, Benrahou K (2020) Investigation on hygro-thermal vibration of P-FG and symmetric S-FG nanobeam using integral Timoshenko beam theory. Adv Nano Res 8(4):293–305
15. Chikr SC, Kaci A, Bousahla AA, Bourada F, Tounsi A, Bedia E, Mahmoud S, Benrahou KH, Tounsi A (2020) A novel four-unknown integral model for buckling response of FG sandwich plates resting on elastic foundations under various boundary conditions using Galerkin's approach. Geomechan Eng 21(5):471–487
16. Refrafi S, Bousahla AA, Bouhadra A, Menasria A, Bourada F, Tounsi A, Bedia E, Mahmoud S, Benrahou KH, Tounsi A (2020) Effects of hygro-thermo-mechanical conditions on the buckling of FG sandwich plates resting on elastic foundations. Computers Concrete 25(4):311–325
17. Bousahla AA, Bourada F, Mahmoud S, Tounsi A, Algarni A, Bedia E, Tounsi A (2020) Buckling and dynamic behavior of the simply supported CNT-RC beams using an integral-first shear deformation theory. Computers Concrete 25(2):155–166
18. Bellal M, Hebali H, Heireche H, Bousahla AA, Tounsi A, Bourada F, Mahmoud S, Bedia E, Tounsi A (2020) Buckling behavior of a single-layered graphene sheet resting on viscoelastic medium via nonlocal four-unknown integral model. Steel Comp Str 34(5):643–655
19. Kaddari M, Kaci A, Bousahla AA, Tounsi A, Bourada F, Bedia EA, Al-Osta MA (2020) A study on the structural behaviour of functionally graded porous plates on elastic foundation using a new quasi-3D model: Bending and free vibration analysis. Computers Concrete 25(1):37
20. Tounsi A, Al-Dulaijan S, Al-Osta MA, Chikh A, Al-Zahrani M, Sharif A, Tounsi A (2020) A four variable trigonometric integral plate theory for hygro-thermo-mechanical bending analysis of AFG ceramic-metal plates resting on a two-parameter elastic foundation. Steel Comp Struc 34(4):511
21. Addou FY, Meradjah M, Bousahla AA, Benachour A, Bourada F, Tounsi A, Mahmoud S (2019) Influences of porosity on dynamic response of FG plates resting on Winkler/Pasternak/Kerr foundation using quasi 3D HSDT. Computers Concrete 24(4):347–367
22. Chaabane LA, Bourada F, Sekkal M, Zerouati S, Zaoui FZ, Tounsi A, Derras A, Bousahla AA, Tounsi A (2019) Analytical study of bending and free vibration responses of functionally graded beams resting on elastic foundation. Struc Eng Mechan 71(2):185–196
23. Mahmoudi A, Benyoucef S, Tounsi A, Benachour A, Adda Bedia EA, Mahmoud S (2019) A refined quasi-3D shear deformation theory for thermo-mechanical behavior of functionally graded sandwich plates on elastic foundations. J Sandwich Struc Mater 21(6):1906–1929
24. Al-Furjan MSH, Habibi M, Dw J, Sadeghi S, Safarpour H, Tounsi A, Chen G (2020) A computational framework for propagated waves in a sandwich doubly curved nanocomposite panel. Eng Computers. https://doi.org/10.1007/s00366-020-01130-8
25. Sahmani S, Fattahi A, Ahmed N (2019) Analytical mathematical solution for vibrational response of postbuckled laminated FG-GPLRC nonlocal strain gradient micro-/nanobeams. Eng Computers 35(4):1173–1189
26. Khiloun M, Bousahla AA, Kaci A, Bessaim A, Tounsi A, Mahmoud S (2019) Analytical modeling of bending and vibration of thick advanced composite plates using a four-variable quasi 3D HSDT. Eng Computers 36(3):807–21. https://doi.org/10.1007/s00366-019-00732-1
27. Sahmani S, Fattahi A, Ahmed N (2019) Analytical treatment on the nonlocal strain gradient vibrational response of postbuckled functionally graded porous micro-/nanoplates reinforced with GPL. Eng Computers 1–20. https://doi.org/10.1007/s00366-019-00782-5
28. Khiloun M, Bousahla AA, Kaci A, Bessaim A, Tounsi A, Mahmoud S (2020) Analytical modeling of bending and vibration of thick advanced composite plates using a four-variable quasi 3D HSDT. Eng Computers 36(3):807–821
29. Oyarhossein M, Khiali V, Hosseinmostofi K, Adineh M, Bayatghiasi H (2019) Numerical study of the gap at the base of the bridge on the river flow parameters. 8(8):264–268. https://mpra.ub.uni-muenchen.de/id/eprint/95406
30. Gao W, Qin Z, Chu F (2020) Wave propagation in functionally graded porous plates reinforced with graphene platelets. Aerospace Sci Technol 12:105860. https://doi.org/10.1016/j.ast.2020.105860
31. Ebrahimi F, Barati MR, Dabbagh A (2016) A nonlocal strain gradient theory for wave propagation analysis in temperature-dependent inhomogeneous nanoplates. Int J Eng Sci 107:169–182

32. Safaei B, Moradi-Dastjerdi R, Qin Z, Behdinan K, Chu F (2019) Determination of thermoelastic stress wave propagation in nanocomposite sandwich plates reinforced by clusters of carbon nanotubes. J Sandwich Struct Mater 10:99636219848282
33. Menasria A, Kaci A, Bousahla AA, Bourada F, Tounsi A, Benrahou KH, Tounsi A, Bedia EA, Mahmoud S (2020) A four-unknown refined plate theory for dynamic analysis of FG-sandwich plates under various boundary conditions. Steel Comp Struct 36(3):355
34. Zine A, Bousahla AA, Bourada F, Benrahou KH, Tounsi A, Adda Bedia E, Mahmoud S, Tounsi A (2020) Bending analysis of functionally graded porous plates via a refined shear deformation theory. Computers Concrete 26(1):63–74
35. Belbachir N, Bourada M, Draiche K, Tounsi A, Bourada F, Bousahla AA, Mahmoud S (2020) Thermal flexural analysis of anti-symmetric cross-ply laminated plates using a four variable refined theory. Smart Struct Syst 25(4):409–422
36. Rahmani MC, Kaci A, Bousahla AA, Bourada F, Tounsi A, Bedia E, Mahmoud S, Benrahou KH, Tounsi A (2020) Influence of boundary conditions on the bending and free vibration behavior of FGM sandwich plates using a four-unknown refined integral plate theory. Computers Concrete 25(3):225–244
37. Boussoula A, Boucham B, Bourada M, Bourada F, Tounsi A, Bousahla A, Tounsi A (2019) A simple nth-order shear deformation theory for thermomechanical bending analysis of different configurations of FG sandwich plates. Smart Struct Syst
38. Abualnour M, Chikh A, Hebali H, Kaci A, Tounsi A, Bousahla AA, Tounsi A (2019) Thermomechanical analysis of antisymmetric laminated reinforced composite plates using a new four variable trigonometric refined plate theory. Computers Concrete 24(6):489–498
39. Belbachir N, Draich K, Bousahla AA, Bourada M, Tounsi A, Mohammadimehr M (2019) Bending analysis of anti-symmetric cross-ply laminated plates under nonlinear thermal and mechanical loadings. Steel Comp Struct 33(1):81–92
40. Sahla M, Saidi H, Draiche K, Bousahla AA, Bourada F, Tounsi A (2019) Free vibration analysis of angle-ply laminated composite and soft core sandwich plates. Steel Comp Struct 33(5):663
41. Balubaid M, Tounsi A, Dakhel B, Mahmoud S (2019) Free vibration investigation of FG nanoscale plate using nonlocal two variables integral refined plate theory. Computers Concrete 24(6):579–586
42. Boutaleb S, Benrahou KH, Bakora A, Algarni A, Bousahla AA, Tounsi A, Tounsi A, Mahmoud S (2019) Dynamic analysis of nanosize FG rectangular plates based on simple nonlocal quasi 3D HSDT. Adv Nano Res 7(3):191
43. Zarga D, Tounsi A, Bousahla AA, Bourada F, Mahmoud S (2019) Thermomechanical bending study for functionally graded sandwich plates using a simple quasi-3D shear deformation theory. Steel Comp Struct 32(3):389–410
44. Ebrahimi F, Sedighi SB (2020) Wave dispersion characteristics of a rectangular sandwich composite plate with tunable magneto-rheological fluid core rested on a visco-Pasternak foundation. Mech Based Design Struct Mach 28:1–4. https://doi.org/10.1080/15397734.2020.1716244
45. Faroughi S, Rahmani A, Friswell M (2020) On wave propagation in two-dimensional functionally graded porous rotating nanobeams using a general nonlocal higher-order beam model. Appl Math Model 80:169–190
46. Liu C, Yu J, Xu W, Zhang X, Zhang B (2020) Theoretical study of elastic wave propagation through a functionally graded microstructured plate base on the modified couple-stress theory. Meccanica 1:1–5. https://doi.org/10.1007/s11012-020-01156-8
47. Ebrahimi F, Barati MR, Haghi P (2017) Thermal effects on wave propagation characteristics of rotating strain gradient temperature-dependent functionally graded nanoscale beams. J Therm Stress 40(5):535–547
48. Barati MR (2017) On wave propagation in nanoporous materials. Int J Eng Sci 116:1–11. https://doi.org/10.1016/j.ijengsci.2017.03.007
49. Moayedi H, Hayati S (2018) Applicability of a CPT-based neural network solution in predicting load-settlement responses of bored pile. Int J Geomech. https://doi.org/10.1061/(ASCE)GM.1943-5622.0001125
50. Moayedi H, Bui DT, Foong LK (2019) Slope stability monitoring using novel remote sensing based fuzzy logic. Sensors. https://doi.org/10.3390/s19214636
51. Moayedi H, Bui DT, Kalantar B, Osouli A, Gör M, Pradhan B, Nguyen H, Rashid ASA (2019) Harris hawks optimization: A novel swarm intelligence technique for spatial assessment of landslide susceptibility. Sensors. https://doi.org/10.3390/s19163590
52. Moayedi H, Mu'azu MA, Kok Foong L, (2019) Swarm-based analysis through social behavior of grey wolf optimization and genetic programming to predict friction capacity of driven piles. Eng Computers. https://doi.org/10.1007/s00366-019-00885-z
53. Moayedi H, Osouli A, Nguyen H, Rashid ASA (2019) A novel Harris hawks' optimization and k-fold cross-validation predicting slope stability. Eng Computers. https://doi.org/10.1007/s00366-019-00828-8
54. Yuan C, Moayedi H (2019) The performance of six neural-evolutionary classification techniques combined with multi-layer perception in two-layered cohesive slope stability analysis and failure recognition. Eng Computers. https://doi.org/10.1007/s00366-019-00791-4
55. Yuan C, Moayedi H (2019) Evaluation and comparison of the advanced metaheuristic and conventional machine learning methods for the prediction of landslide occurrence. Eng Computers. https://doi.org/10.1007/s00366-019-00798-x
56. Li C, Han Q, Wang Z, Wu X (2020) Analysis of wave propagation in functionally graded piezoelectric composite plates reinforced with graphene platelets. Appl Mathem Model
57. Ebrahimi F, Dabbagh A (2018) Thermo-magnetic field effects on the wave propagation behavior of smart magnetostrictive sandwich nanoplates. Eur Phys J Plus 133(3):97
58. Abad F, Rouzegar J (2019) Exact wave propagation analysis of moderately thick Levy-type plate with piezoelectric layers using spectral element method. Thin Walled Struct 141:319–331
59. Habibi M, Mohammadgholiha M, Safarpour H (2019) Wave propagation characteristics of the electrically GNP-reinforced nanocomposite cylindrical shell. J Brazilian Soc Mech Sci Eng 41(5):221. https://doi.org/10.1007/s40430-019-1715-x
60. Zhao X, Li D, Yang B, Ma C, Zhu Y, Chen H (2014) Feature selection based on improved ant colony optimization for online detection of foreign fiber in cotton. Appl Soft Comp 24:585–596
61. Wang M, Chen H (2020) Chaotic multi-swarm whale optimizer boosted support vector machine for medical diagnosis. Appl Soft Comp 88:105946
62. Zhao X, Zhang X, Cai Z, Tian X, Wang X, Huang Y, Chen H, Hu L (2019) Chaos enhanced grey wolf optimization wrapped ELM for diagnosis of paraquat-poisoned patients. Comput Biol Chem 78:481–490
63. Xu X, Chen H-L (2014) Adaptive computational chemotaxis based on field in bacterial foraging optimization. Soft Comput 18(4):797–807
64. Shen L, Chen H, Yu Z, Kang W, Zhang B, Li H, Yang B, Liu D (2016) Evolving support vector machines using fruit fly optimization for medical data classification. Knowledge Based Syst 96:61–75
65. Wang M, Chen H, Yang B, Zhao X, Hu L, Cai Z, Huang H, Tong C (2017) Toward an optimal kernel extreme learning machine

using a chaotic moth-flame optimization strategy with applications in medical diagnoses. Neurocomputing 267:69–84
66. Xu Y, Chen H, Luo J, Zhang Q, Jiao S, Zhang X (2019) Enhanced Moth-flame optimizer with mutation strategy for global optimization. Inform Sci 492:181–203
67. Chen H, Zhang Q, Luo J, Xu Y, Zhang X (2020) An enhanced Bacterial Foraging Optimization and its application for training kernel extreme learning machine. Appl Soft Comp 86:105884
68. Bakhtiari M, Tarkashvand A, Daneshjou K (2020) Plane-strain wave propagation of an impulse-excited fluid-filled functionally graded cylinder containing an internally clamped shell. Thin-Walled Structures 5:106482. https://doi.org/10.1016/j.tws.2019.106482
69. Ebrahimi F, Mohammadi K, Barouti MM, Habibi M (2019) Wave propagation analysis of a spinning porous graphene nanoplatelet-reinforced nanoshell. Waves in Random and Complex Media:1–27
70. Ebrahimi F, Seyfi A (2019) Wave propagation response of multi-scale hybrid nanocomposite shell by considering aggregation effect of CNTs. Mech Based Design Struct Mach 24:1–22. https://doi.org/10.1080/15397734.2019.1666722
71. Karami B, Shahsavari D, Janghorban M, Dimitri R, Tornabene F (2019) Wave propagation of porous nanoshells. Nanomaterials 9(1):22
72. Farhangi V, Karakouzian M, Geertsema M (2020) Effect of Micropiles on Clean Sand Liquefaction Risk Based on CPT and SPT. Appl Sci 10(9):3111
73. Farhangi V, Karakouzian M (2019) Design of Bridge Foundations Using Reinforced Micropiles. In: Proceedings of the International Road Federation Global R2T Conference & Expo, Las Vegas, NV, USA, pp 19–22
74. Farhangi V, Karakouzian M (2020) Effect of fiber reinforced polymer tubes filled with recycled materials and concrete on structural capacity of pile foundations. Appl Sci 10(5):1554
75. Tornabene F, Bacciocchi M, Fantuzzi N, Reddy J (2019) Multiscale approach for three-phase CNT/polymer/fiber laminated nanocomposite structures. Polym Compos 40(S1):E102–E126. https://doi.org/10.1002/pc.24520
76. Shariati A, Habibi M, Tounsi A, Safarpour H, Safa M (2020) Application of exact continuum size-dependent theory for stability and frequency analysis of a curved cantilevered microtubule by considering viscoelastic properties. Eng Computers. https://doi.org/10.1007/s00366-020-01024-9
77. Li J, Tang F, Habibi M (2020) Bi-directional thermal buckling and resonance frequency characteristics of a GNP-reinforced composite nanostructure. Eng Computers. https://doi.org/10.1007/s00366-020-01110-y
78. Moayedi H, Ebrahimi F, Habibi M, Safarpour H, Foong LK (2020) Application of nonlocal strain–stress gradient theory and GDQEM for thermo-vibration responses of a laminated composite nanoshell. Eng Computers. https://doi.org/10.1007/s00366-020-01002-1
79. Ebrahimi F, Mahesh V (2019) Chaotic dynamics and forced harmonic vibration analysis of magneto-electro-viscoelastic multiscale composite nanobeam. Eng Computers 3:1–4. https://doi.org/10.1007/s00366-019-00865-3
80. Al-Furjan M, Safarpour H, Habibi M, Safarpour M, Tounsi A (2020) A comprehensive computational approach for nonlinear thermal instability of the electrically FG-GPLRC disk based on GDQ method. Eng Computers 5:1–25
81. Gholipour A, Ghayesh MH, Hussain S (2020) A continuum viscoelastic model of Timoshenko NSGT nanobeams. Eng Computers 23:1–8. https://doi.org/10.1007/s00366-020-01088-7
82. Moayedi H, Darabi R, Ghabussi A, Habibi M, Foong LK (2020) Weld orientation effects on the formability of tailor welded thin steel sheets. Thin Walled Struct 149:106669
83. Shokrgozar A, Ghabussi A, Ebrahimi F, Habibi M, Safarpour H (2020) Viscoelastic dynamics and static responses of a graphene nanoplatelets-reinforced composite cylindrical microshell. Mech Based Design Struct Mach 4:1–28. https://doi.org/10.1080/15397734.2020.1719509
84. Ghabussi A, Marnani JA, Rohanimanesh MS Improving seismic performance of portal frame structures with steel curved dampers. In: Structures, 2020. Elsevier, pp 27–40. https://doi.org/10.1016/j.istruc.2019.12.025
85. Safarpour M, Ghabussi A, Ebrahimi F, Habibi M, Safarpour H (2020) Frequency characteristics of FG-GPLRC viscoelastic thick annular plate with the aid of GDQM. Thin Walled Struct 150:106683
86. Ghabussi A, Habibi M, NoormohammadiArani O, Shavalipour A, Moayedi H, Safarpour H (2020) Frequency characteristics of a viscoelastic graphene nanoplatelet–reinforced composite circular microplate. J Vibr Control. https://doi.org/10.1177/1077546320923930
87. Ghabussi A, Ashrafi N, Shavalipour A, Hosseinpour A, Habibi M, Moayedi H, Babaei B, Safarpour H (2019) Free vibration analysis of an electro-elastic GPLRC cylindrical shell surrounded by viscoelastic foundation using modified length-couple stress parameter. Mech Based Design Struct Mach 1–25
88. Shariati A, Ghabussi A, Habibi M, Safarpour H, Safarpour M, Tounsi A, Safa M (2020) Extremely large oscillation and nonlinear frequency of a multi-scale hybrid disk resting on nonlinear elastic foundation. Thin Walled Struct 154:106840. https://doi.org/10.1016/j.tws.2020.106840
89. Jermsittiparsert K, Ghabussi A, Forooghi A, Shavalipour A, Habibi M, won Jung D, Safa M (2020) Critical voltage, thermal buckling and frequency characteristics of a thermally affected GPL reinforced composite microdisk covered with piezoelectric actuator. Mech Based Design Struct Mach. https://doi.org/10.1080/15397734.2020.1748052
90. Al-Furjan M, Habibi M, Chen G, Safarpour H, Safarpour M, Tounsi A (2020) Chaotic oscillation of a multi-scale hybrid nano-composites reinforced disk under harmonic excitation via GDQM. Composite Struct 30:112737. https://doi.org/10.1016/j.compstruct.2020.112737
91. Habibi M, Hashemi R, Sadeghi E, Fazaeli A, Ghazanfari A, Lashini H (2016) Enhancing the mechanical properties and formability of low carbon steel with dual-phase microstructures. J Mater Eng Perf 25(2):382–389
92. Habibi M, Hashemi R, Tafti MF, Assempour A (2018) Experimental investigation of mechanical properties, formability and forming limit diagrams for tailor-welded blanks produced by friction stir welding. J Manuf Processes 31:310–323
93. Al-Furjan M, Habibi M, Safarpour H (2020) Vibration control of a smart shell reinforced by graphene nanoplatelets. Int J Appl Mech. https://doi.org/10.1142/S1758825120500660
94. Liu Z, Su S, Xi D, Habibi M (2020) Vibrational responses of a MHC viscoelastic thick annular plate in thermal environment using GDQ method. Mech Based Design Struct Mach 1–26
95. Shi X, Li J, Habibi M (2020) On the statics and dynamics of an electro-thermo-mechanically porous GPLRC nanoshell conveying fluid flow. Mech Based Design Struct Machines 1–37
96. Habibi M, Safarpour M, Safarpour H (2020) Vibrational characteristics of a FG-GPLRC viscoelastic thick annular plate using fourth-order Runge-Kutta and GDQ methods. Mech Based Design Struct Mach 1–22
97. Zhang X, Shamsodin M, Wang H, NoormohammadiArani O, khan AM, Habibi M, Al-Furjan M (2020) Dynamic information of the time-dependent tobullian biomolecular structure using a high-accuracy size-dependent theory. J Biomol Struct Dynamics 1–26

98. Habibi M, Taghdir A, Safarpour H (2019) Stability analysis of an electrically cylindrical nanoshell reinforced with graphene nanoplatelets. Comp Part B 175:107125
99. Pourjabari A, Hajilak ZE, Mohammadi A, Habibi M, Safarpour H (2019) Effect of porosity on free and forced vibration characteristics of the GPL reinforcement composite nanostructures. Computers Math Appl 77(10):2608–2626
100. Cheshmeh E, Karbon M, Eyvazian A, Jung DW, Habibi M, Safarpour M (2020) Buckling and vibration analysis of FG-CNTRC plate subjected to thermo mechanical load based on higher order shear deformation theory. Mech Based Design Struc Mach 20:1–24. https://doi.org/10.1080/15397734.2020.1744005
101. Najaafi N, Jamali M, Habibi M, Sadeghi S, Jung DW, Nabipour N (2020) Dynamic instability responses of the substructure living biological cells in the cytoplasm environment using stress-strain size-dependent theory. J Biomol Struct Dyn 10(1080/07391102):1751297
102. Shariati A, Mohammad-Sedighi H, Żur KK, Habibi M, Safa M (2020) Stability and dynamics of viscoelastic moving rayleigh beams with an asymmetrical distribution of material parameters. Symmetry 12(4):586
103. Oyarhossein MA, Aa A, Habibi M, Makkiabadi M, Daman M, Safarpour H, Jung DW (2020) Dynamic response of the nonlocal strain-stress gradient in laminated polymer composites microtubes. Sci Rep 10(1):5616. https://doi.org/10.1038/s41598-020-61855-w
104. Shamsaddini Lori E, Ebrahimi F, Elianddy Bin Supeni E, Habibi M, Safarpour H (2020) The critical voltage of a GPL-reinforced composite microdisk covered with piezoelectric layer. Eng Computers. https://doi.org/10.1007/s00366-020-01004-z
105. Safarpour M, Ebrahimi F, Habibi M, Safarpour H (2020) On the nonlinear dynamics of a multi-scale hybrid nanocomposite disk. Eng Computers 22:1–20. https://doi.org/10.1007/s00366-020-00949-5
106. Ebrahimi F, Supeni EEB, Habibi M, Safarpour H (2020) Frequency characteristics of a GPL-reinforced composite microdisk coupled with a piezoelectric layer. Eur Phys J Plus 135(2):144
107. Ebrahimi F, Hashemabadi D, Habibi M, Safarpour H (2020) Thermal buckling and forced vibration characteristics of a porous GNP reinforced nanocomposite cylindrical shell. Microsyst Technol 26(2):461–73. https://doi.org/10.1007/s00542-019-04542-9
108. Adamian A, Safari KH, Sheikholeslami M, Habibi M, Al-Furjan M, Chen G (2020) Critical temperature and frequency characteristics of gpls-reinforced composite doubly curved panel. Appl Sci 10(9):3251
109. Shariati A, Habibi M, Tounsi A, Safarpour H, Safa M (2020) Application of exact continuum size-dependent theory for stability and frequency analysis of a curved cantilevered microtubule by considering viscoelastic properties. Eng Computers. https://doi.org/10.1007/s00366-020-01024-9
110. Ghayesh MH (2019) Dynamical analysis of multilayered cantilevers. Commun Nonlinear Sci Numer Simul 71:244–253
111. Farokhi H, Ghayesh MH, Gholipour A (2017) Dynamics of functionally graded micro-cantilevers. Int J Eng Sci 115:117–130
112. Ghayesh MH (2018) Dynamics of functionally graded viscoelastic microbeams. Int J Eng Sci 124:115–131
113. Ghayesh MH, Farokhi H (2020) Extremely large dynamics of axially excited cantilevers. Thin-Walled Structures:106275
114. Ghayesh MH (2019) Mechanics of viscoelastic functionally graded microcantilevers. Eur J Mech A/Solids 73:492–499
115. Reddy JN (2003) Mechanics of laminated composite plates and shells: theory and analysis. CRC press
116. Shariati A, Bayrami SS, Ebrahimi F, Toghroli A (2020) Wave propagation analysis of electro-rheological fluid-filled sandwich composite beam. Mech Based Design Struc Mach 28:1–10. https://doi.org/10.1080/15397734.2020.1745646
117. Habibi M, Mohammadi A, Safarpour H, Shavalipour A, Ghadiri M (2019) Wave propagation analysis of the laminated cylindrical nanoshell coupled with a piezoelectric actuator. Mech Based Design Struc Mach 2:1–9. https://doi.org/10.1080/15397734.2019.1697932
118. Shariati A, Mohammad-Sedighi H, Żur KK, Habibi M, Safa M (2020) On the vibrations and stability of moving viscoelastic axially functionally graded nanobeams. Materials 13(7):1707
119. Moayedi H, Habibi M, Safarpour H, Safarpour M, Foong L. Buckling and frequency responses of a graphen nanoplatelet reinforced composite microdisk. Int J Appl Mech
120. Moayedi H, Aliakbarlou H, Jebeli M, Noormohammadiarani O, Habibi M, Safarpour H, Foong L (2020) Thermal buckling responses of a graphene reinforced composite micropanel structure. Int J Appl Mech 12(01):2050010
121. Shokrgozar A, Safarpour H, Habibi M (2020) Influence of system parameters on buckling and frequency analysis of a spinning cantilever cylindrical 3D shell coupled with piezoelectric actuator. Proc Inst Mech Eng Part C 234(2):512–529
122. Habibi M, Mohammadi A, Safarpour H, Ghadiri M (2019) Effect of porosity on buckling and vibrational characteristics of the imperfect GPLRC composite nanoshell. Mechan Based Design Struc Mach 17:1–30. https://doi.org/10.1080/15397734.2019.1701490
123. Nadri S, Xie L, Jafari M, Alijabbari N, Cyberey ME, Barker NS, Lichtenberger AW, Weikle RM (2018) A 160 GHz frequency Quadrupler based on heterogeneous integration of GaAs Schottky diodes onto silicon using SU-8 for epitaxy transfer. In: 2018 IEEE/MTT-S International Microwave Symposium-IMS, IEEE, pp 769–772
124. Ebrahimi F, Dabbagh A (2019) Vibration analysis of multi-scale hybrid nanocomposite plates based on a Halpin-Tsai homogenization model. Compos Part B Eng 173:106955
125. Wattanasakulpong N, Chaikittiratana A (2015) Exact solutions for static and dynamic analyses of carbon nanotube-reinforced composite plates with Pasternak elastic foundation. Appl Math Model 39(18):5459–5472. https://doi.org/10.1016/j.apm.2014.12.058